Strategies for enhancing the heterogeneous Fenton catalytic reactivity: A review

Yanping Zhu[a,b,d], Runliang Zhu[a,*], Yunfei Xi[c,d,**], Jianxi Zhu[a], Gangqiang Zhu[e], Hongping He[a]

[a] CAS Key Laboratory of Mineralogy and Metallogeny, Guangdong Provincial Key Laboratory of Mineral Physics and Materials, Guangzhou Institute of Geochemistry, Chinese Academy of Sciences(CAS), Guangzhou, 510640, China
[b] University of Chinese Academy of Sciences, Beijing, 100049, China
[c] School of Earth, Environmental and Biological Sciences, Queensland University of Technology (QUT), Brisbane, QLD, 4001, Australia
[d] Institute for Future Environments and Science and Engineering Faculty, Queensland University of Technology (QUT), Brisbane, QLD, 4001, Australia
[e] School of physics and information technology, Shaanxi Normal University, Xi'an, 710062, China

ARTICLE INFO

ABSTRACT

Heterogeneous Fenton reactions have gained widespread attention in removing recalcitrant organic contaminants as the reaction between solid Fenton catalysts and H_2O_2 can generate highly reactive hydroxyl radicals (HO˙). However, several drawbacks, such as the low-speed generation of Fe(II), high consumption of H_2O_2, and acidic reaction conditions (generally at ˜ pH 3), are always the core issues that hamper the large-scale application of heterogeneous Fenton reactions in environmental remediation. Thus, a large number of studies have been devoted to tackling these drawbacks, and this paper intends to comprehensively review the developed strategies for enhancing heterogeneous Fenton reactivity, mainly over the last decade. Based on a comprehensive survey of previous studies, we categorize these strategies according to their reaction mechanisms. For example, introducing additional electrons (e.g., from external electric fields, electron-rich materials, semiconductors, plasmonic materials, or doped metals) to heterogeneous Fenton catalysts can accelerate the generation of Fe(II); the in situ generation of H_2O_2 can be achieved by combining ultrasound, electricity, semiconductors, and iron-based catalysts in the system; and controlling the specific morphologies and exposed facets of heterogeneous Fenton catalysts can greatly promote the decomposition of H_2O_2. In addition, we briefly introduce some recent novel heterogeneous Fenton-like reactions that are of particular interest, including constructing dual reaction centers (i.e., the electron-poor center and the electron-rich center) and synthesizing single-atom catalysis-based heterogeneous Fenton-like catalysts. Moreover, this review article analyzes and compares the merits of each strategy for enhancing heterogeneous Fenton/Fenton-like reactions. We believe this review can motivate the construction of novel and efficient heterogeneous Fenton/Fenton-like systems and help readers choose proper Fenton/Fenton-like reaction systems for industrial applications.

1. Introduction

With the rapid development of urbanization and industrialization, environmental pollution caused by the unabated release of toxic agents into water has become an overwhelming issue worldwide, particularly in developing and underdeveloped countries [1]. A variety of contaminants, such as industrial dyes, pharmaceuticals, and agrochemicals widely exist in wastewater, rivers, and groundwater, which are capable of directly or indirectly affecting living organisms, including humans [2,3]. Various methods have been developed to deal with contaminated water, such as adsorption, flocculation, biological methods, and advanced oxidation processes (AOPs) [4]. Among these methods, AOPs have shown great potential to convert most organic pollutants to smaller compounds and even to CO_2, owing to the highly effective reactive oxygen species (ROS) generated during the reaction process [5,6].

The Fenton process is one of the most cost-effective AOPs [7–9]. Since Henry J. Fenton found that H_2O_2 can be activated by Fe^{2+} to oxidize tartaric acid, Fenton and its related reactions have drawn great interest in wastewater treatment [10]. Highly active hydroxyl radicals (HO˙) can be generated by the reaction between Fe^{2+} and H_2O_2 (Eq. 1), and the formed Fe^{3+} can be reduced by H_2O_2 to regenerate Fe^{2+}

Table 1
The main steps of the Fenton reaction process.

	Reactions	Rate constant (M^{-1} s^{-1})
Chain initiation steps	$Fe^{2+} + H_2O_2 \rightarrow Fe^{3+} + HO^{\cdot} + OH^{-}$	$40 - 80$ [27]
	$Fe^{3+} + H_2O_2 \rightarrow Fe^{2+} + HO_2^{\cdot} + H^{+}$	$0.001 - 0.01$ [16]
	$HO_2^{\cdot} \rightarrow H^{+} + O_2^{\cdot -}$	(pKa = 4.8) [16]
Chain propagation steps	$H_2O_2 + HO^{\cdot} \rightarrow HO_2^{\cdot} + H_2O$	$(1.7 - 4.5) \times 10^7$ [27]
	$H_2O_2 + HO_2^{\cdot} \rightarrow O_2 + H_2O + HO^{\cdot}$	0.5, 3 [27]
	$H_2O_2 + O_2^{\cdot -} \rightarrow O_2 + HO^{\cdot} + OH^{-}$	16, 0.13 [27]
	$RH + HO^{\cdot} \rightarrow R^{\cdot} + H_2O$	$>10^8 - 10^9$ [21]
	$R^{\cdot} + O_2 \rightarrow RO_2^{\cdot}$	/
	$R^{\cdot} + Fe^{2+} \rightarrow RH + Fe^{3+}$	/
	$R^{\cdot} + Fe^{3+} \rightarrow R^{+} + Fe^{2+}$	/
Chain termination steps	$Fe^{3+} + HO_2^{\cdot} \rightarrow Fe^{2+} + O_2 + H^{+}$	3.3×10^7 [21]
	$Fe^{2+} + HO^{\cdot} \rightarrow Fe^{3+} + OH^{-}$	3.2×10^8 [9]
	$HO^{\cdot} + HO^{\cdot} \rightarrow H_2O_2$	5.2×10^9 [21]
	$2HO^{\cdot} + 2HO^{\cdot} \rightarrow O_2 + 2H_2O$	7.15×10^9 [9]
	$HO_2^{\cdot} + HO_2^{\cdot} \rightarrow O_2 + H_2O_2$	2.3×10^6 [21]
	$HO_2^{\cdot} + HO^{\cdot} \rightarrow O_2 + H_2O$	7.1×10^9 [21]
	$R^{\cdot} + R^{\cdot} \rightarrow R\text{-}R$	/

through Eq. 2. With a high redox potential ($E^0(HO^{\cdot}/H_2O) = 2.73$ V), $HO^{\cdot}$ can powerfully degrade most organic contaminants in a non-selective way [11]. Even so, the applications of homogeneous Fenton reactions are hampered mainly due to the following drawbacks: (i) large consumption of H_2O_2; (ii) narrow range of optimum pH values (pH ~ 3); and (iii) excessive amounts of generated ferric hydroxide sludge [12].

$$Fe^{2+} + H_2O_2 \rightarrow Fe^{3+} + HO^{\cdot} + OH^{-} \qquad (1)$$

$$Fe^{3+} + H_2O_2 \rightarrow Fe^{2+} + HO_2^{\cdot} + H^{+} \qquad (2)$$

$$\equiv Fe(III) + H_2O_2 \rightarrow \equiv Fe(II) + HO_2^{\cdot} + H^{+} \qquad (3)$$

$$\equiv Fe(II) + H_2O_2 \rightarrow \equiv Fe(III) + HO^{\cdot} + OH^{-} \qquad (4)$$
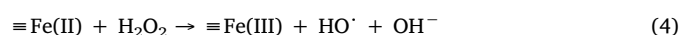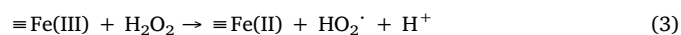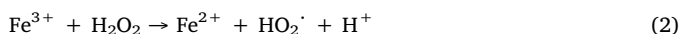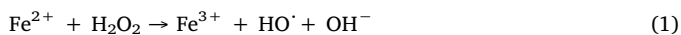
To avoid the generation of ferric hydroxide sludge and circumvent the effect of limited pH range on homogeneous Fenton reactions, many researchers have gradually begun to pay attention to heterogeneous Fenton catalysis [12–14]. In heterogeneous catalysis, iron is stabilized within the catalyst's structure and can effectively produce $HO^{\cdot}$ from the excitation of H_2O_2 without iron hydroxide precipitation [3,14]. There are two main reaction routes between heterogeneous catalysts and H_2O_2: (i) the reaction of unavoidably leached Fe from catalysts with H_2O_2 (i.e., a homogeneous Fenton reaction) (Eqs. 1–2), and (ii) the reaction of surface Fe ($\equiv$Fe(III)) with H_2O_2 (Eqs. 3–4) [15,16].

In most of these heterogeneous catalysts, iron mainly exists in the form of Fe(III). Therefore, in the traditional heterogeneous Fenton reaction, the redox cycling of Fe(III)/Fe(II) and Fe^{3+}/Fe^{2+} by H_2O_2 is critical to keep the Fenton reactions continuous. However, as compared with the reactions between Fe^{2+}/Fe(II) and H_2O_2, the reduction of Fe^{3+}/Fe(III) by H_2O_2 (Eqs. 2,3) are always the rate-limiting steps due to the low rate constant (0.001–0.01 M^{-1} s^{-1}), which determines the overall efficiency of the whole Fenton reactions. In addition, in these two steps, H_2O_2 is decomposed to hydroperoxyl radical ($HO_2^{\cdot}$) [17], which can also participate in the degradation of contaminants. However, compared to $HO^{\cdot}$, $HO_2^{\cdot}$ is less reactive ($E^0(HO_2^{\cdot}/H_2O_2) = 1.50$ V). Therefore, how to accelerate the redox cycling of Fe(III)/Fe(II) and promote the utilization efficiency of H_2O_2 in traditional heterogeneous Fenton reactions is the core issue, motivating researchers to design more effective heterogeneous Fenton catalysts and reaction strategies.

Accordingly, many strategies have been developed to accelerate the redox cycling of Fe(III)/Fe(II), improving the utilization efficiency of H_2O_2, broadening the pH range, and promoting the stability of catalysts in the heterogeneous Fenton process. Based on the promising applications and extensive studies of heterogeneous Fenton reaction systems, a number of review papers regarding this research area have been published in the past decade, which involve one or several of the following aspects: the essential effect parameters (e.g., pH, H_2O_2 dosage, catalyst dosage, and temperature) [7,18,19], the fundamental reaction mechanisms [15,20], different types of heterogeneous Fenton catalysts [3,6,9,14,21–24], and the degradation of specific contaminants [12,25,26]. This review paper, for the first time, intends to systematically compile the research progress on resolving the drawbacks in heterogeneous Fenton reactions, particularly focusing on the strategies and their underlying mechanisms for enhancing heterogeneous Fenton reactivity. We believe that this review paper can motivate the construction of novel and efficient heterogeneous Fenton/Fenton-like systems and help readers choose proper Fenton/Fenton-like reaction systems for industrial applications.

2. Basic knowledge of Fenton and heterogeneous Fenton reactions

In a traditional homogeneous Fenton reaction, the process is very complex and includes a chain of reactions, which can be classified into three general chain steps: initiation, propagation, and termination reactions (Table 1) [9,27]. These steps include (i) production of ROS, such as $HO^{\cdot}$, $HO_2^{\cdot}$, and superoxide radical ($O_2^{\cdot -}$), which initiate the oxidation reactions; (ii) propagation of ROS, reactions of ROS with organic compounds to generate alkyl radicals ($R^{\cdot}$) and alkyl peroxyl radical ($RO_2^{\cdot}$), and their further transformations; and (iii) termination of reactive intermediates [27]. In a Fenton reaction system, how to take advantage of the initiation and propagation reactions and avoid those undesirable termination reactions is still a considerable challenge.

Many homogeneous Fenton systems have been reported for the efficient degradation of various contaminants according to the above efficient reactions [10,19]. However, in practical industrial applications, the complexity and quantity of pollutants are relatively high, therefore, a large number of Fe^{2+} (18–410 mmol/L) and H_2O_2 (30–6000 mmol/L) are generally required to produce sufficient $HO^{\cdot}$ for wastewater treatment to meet the discharge standard, which is a major barrier to the application of this treatment [28]. In addition, the reactivity of Fe^{2+} is significantly affected by solution pH. When the pH is above 3, Fe^{2+} starts to form $Fe(OH)_2$, and the content of $Fe(OH)_2$ increases dramatically until it reaches a plateau at about pH 4 [10]. The formed $Fe(OH)_2$ is approximately 10 times more reactive than Fe^{2+} [10], resulting in a maximum reactivity of ferrous iron species at pH 4. However, Fe^{3+} is gradually generated in the reaction of Eq. (1). Moreover, Fe^{3+} begins to precipitate above pH 3 in the form of relatively inactive hydrous oxyhydroxides. Considering the above factors, the rates of homogeneous Fenton reactions usually reach the maximum at pH 3. Therefore, large amounts of acid (usually sulfuric acid) are needed to maintain the pH of ~ 3. After the process, the effluent needs

Table 2

The common heterogeneous Fenton catalysts (montmorillonite: Mt; granular activated carbon: GAC).

Catalysts/Substrate	Classification	Examples	References
Iron minerals	Magnetite	$Zn/Co/Mo-Fe_3O_4$, Fe^0/Fe_3O_4, GO/Fe_3O_4, $Fe_3O_4@void@TiO_2$	[9,30,31,32,33,34]
	Ferrihydrite	Ag/AgX(X = Cl, Br)/Fh, $BiVO_4$/Fh, Citrate/Fh, Fullerol/Fh	[11,16,35,36,37]
	Hematite	S, $N-\alpha-Fe_2O_3$, $\alpha-Fe_2O_3/Bi_2WO_6$, different facet-controlled hematite, $Ag/\alpha-Fe_2O_3$	[38,39,40,41,42]
	Goethite	$Cu-\alpha-FeOOH$, $rGO-\alpha-FeOOH$, $Cu-Fe_3O_4@FeOOH$, $FeOOH/g-C_3N_4$	[43,44,45,46,47,81]
	Akaganèite	$CNTs/\beta-FeOOH$, $\beta-FeOOH/GO$, $TiO_2/\beta-FeOOH$	[48,49,50]
	Lepidocrocite	$g-C_3N_4/Ag/\gamma-FeOOH$, $\gamma-FeOOH-GAC$	[51,52]
	Maghemite	$\gamma-Fe_2O_3$/oxalate, $\alpha-FeOOH/\gamma-Fe_2O_3$	[53,54]
	Pyrite	FeS_2/SiO_2	[55,56,57,58]
	Schwertmannite	TiO_2/Sh	[59,60,61,62]
	Pseudobrookite	$TiO_2/Fe_2TiO_5/Fe_2O_3$	[63]
Clay-based catalysts	Layered double hydroxides	Co/Fe-LDHs, Cu/Fe-LDHs, Ni/Fe-LDHs	[64,65,66]
	Pillared clays	Fe/Mt, Fe-Al/Mt, Cu-Al/Mt	[24,67,68]
	Clay-supported catalysts	Fe/bentonite, Fe/laponite, Ag/AgCl/Fe-Sepiolite, Ag_3PO_4/Fe-Mt, $BiVO_4$/Fe-Mt	[67,68,69,70,71,72]
Other iron-containing catalysts	Nano zero-valent iron	Biochar/nZVI, $CNTs-Fe^0$, $Fe@Fe_2O_3$, nZVI-diatomite	[73,74,75,76,77,78]
	Transition metal-exchanged zeolites	Fe, Mn, Cu-zeolites	[79,80]
	$Bi_xFe_yO_z$	$Bi_{25}FeO_{40}$, $BiFeO_3/g-C_3N_4$	[82,83,84,85,86]
	$ZnFe_2O_4$	$Ag/ZnO/ZnFe_2O_4$	[87,88]
	$MnFe_2O_4$	$Fe^0@C@MnFe_2O_4$	[89]
	$LaFeO_3$	$Pt/LaFeO_3$	[83,90,91]
	$CuFe_yO_z$	$CuFeO_2$, $CuFe_2O_4$@graphite carbon	[92,93,94]
	$FePO_4$	$GO/FePO_4$, $NCNTs-FePO_4$	[95,96,97]
	$Co_xFe_yO_4$	$Co_xFe_yO_4-BiOBr$, $CoFe_2O_4/g-C_3N_4$	[98,99,100]
	FeOCl	$FeOCl/SiO_2$	[101,102]

to be neutralized with a base before the waste is safely discharged. This treatment gives rise to extra cost and significant amounts of sludge, which represents a serious drawback to the process due to disposal problems [29].

Hence, a great deal of attention has been paid to heterogeneous Fenton catalysts, including iron minerals, Clay-based catalysts, and other iron-containing catalysts (Table 2). Among them, iron minerals mainly include magnetite (Fe_3O_4) [9,30–34], ferrihydrite (Fh, $Fe_5HO_8·4H_2O$) [11,16,35–37], hematite ($\alpha-Fe_2O_3$) [38–42], goethite ($\alpha-FeOOH$) [43–47], akaganèite ($\beta-FeOOH$) [48–50], lepidocrocite ($\gamma-FeOOH$) [51,52], maghemite ($\gamma-Fe_2O_3$) [53,54], pyrite (FeS_2) [55–58], Schwertmannite (Sh, $Fe_8O_8(OH)_{8-x}(SO_4)_x$) [59–62], pseudobrookite (Fe_2TiO_5) [63], etc. Clay-based catalysts include layered double hydroxides (LDHs) [64–66], pillared clays [24,67,68], clay-supported catalysts [67–72], etc. Other iron-containing catalysts mainly contain nano zero-valent iron (nZVI) [73–78], transition metal-exchanged zeolites [79,80], and $Bi_xFe_yO_z$ [92,102–104], etc. In these catalysts, Fe (III) species are "immobilized" within the structure of the catalysts. Therefore, these catalysts can retain their stability to decompose H_2O_2 into $HO^·$, preventing the obvious leaching of iron ions and the generation of iron hydroxide precipitation. Accordingly, these catalysts can be easily recovered after the reaction, remaining high activity after multiple uses [14]. The good stability of these catalysts can also mediate heterogeneous Fenton reactions over a wide range of pH values (even at neutral pH) in the meanwhile [16]. That is why the interests of the scientific community in this subject have increased continuously in the last decade (Fig. 1). However, the development of heterogeneous Fenton catalysis still has many controversial topics or problems. For example, in heterogeneous Fenton catalytic system, whether the dissolved irons or the irons in the solid phase plays the leading role, whether the high-valent iron species (i.e., Fe(IV)) exist, and how to improve the heterogeneous Fenton catalytic activity.

In heterogeneous Fenton catalysis system, it is worth exploring whether the dissolved irons or the irons in the solid phase plays the leading role. It was found that the stability of the catalyst and the presence of strong complexing substances in the heterogeneous Fenton reaction system significantly affected the contribution of homogeneous and heterogeneous Fenton catalysis. For example, in heterogeneous Fenton systems, nZVI can serve as a source of for the continuous dissolution of iron, especially at acidic pH, which contributes to a homogeneous Fenton reaction-dominated mechanism (Eqs. 5–7) [15].
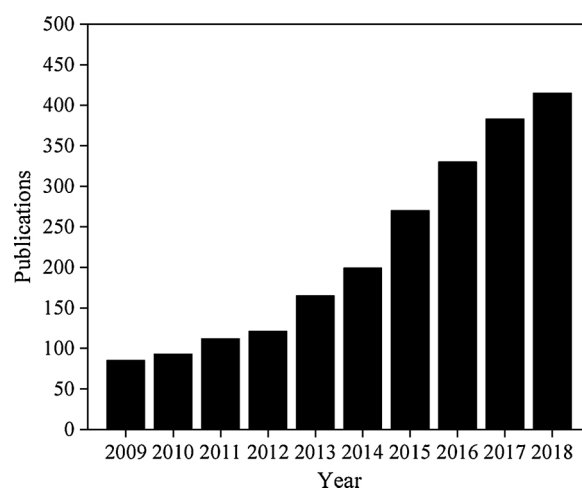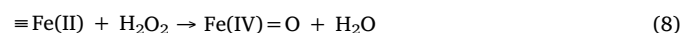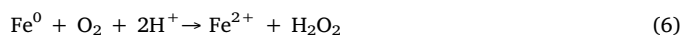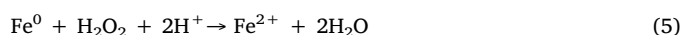

Fig. 1. Evolution of the number of scientific papers devoted to the applications of heterogeneous Fenton processes. Source: Web of Science Core Collection; Topic: together with "Heterogeneous Fenton", "Catalytic Wet Peroxide Oxidation", and "CWPO"; Searching time: April 2019.

Moreover, some iron-complexing ligands (e.g., EDTA) can enhance the solubility of iron catalysts [103], which increases the contribution of homogeneous Fenton reactions. However, most iron-based heterogeneous Fenton catalysts are stable and undergo limited iron leaching during reaction processes, even in acidic solution [11,104]. Hence, it is generally believed that organic contaminants are mainly oxidized by the ROS generated from $\equiv Fe(III)$ or $\equiv Fe(II)$ (i.e., the heterogeneous Fenton reaction rather than the homogenous Fenton reaction) [15,62].

$$Fe^0 + H_2O_2 + 2H^+ \rightarrow Fe^{2+} + 2H_2O \tag{5}$$

$$Fe^0 + O_2 + 2H^+ \rightarrow Fe^{2+} + H_2O_2 \tag{6}$$

$$Fe^0 + 2H^+ \rightarrow Fe^{2+} + H_2 \tag{7}$$

$$\equiv Fe(II) + H_2O_2 \rightarrow Fe(IV)=O + H_2O \tag{8}$$

$$Fe^{2+} + H_2O_2 \rightarrow FeO^{2+} + H_2O \tag{9}$$

In addition, the presence of Fe(IV) is also a controversial issue in heterogeneous reactions. Some studies have reported that in addition to $HO^·$ and $HO_2^·/O_2^{·-}$, (i.e., Fe(IV)) can also be generated in the heterogeneous Fenton system, especially at neutral or basic pH or in the presence of ligands through Eq. (8) [103]. Other researchers have noted that another form of Fe(IV) (i.e., FeO^{2+}) might be generated from the leached iron-induced homogeneous Fenton reaction, most likely through heterolytic O−O bond cleavage by the inner-sphere reaction of Fe^{2+} and H_2O_2 (Eq. 9) [15,105]. Compared with $HO^·$, $HO_2^·/O_2^{·-}$ and Fe(IV) ($E^0(Fe^{4+}/Fe^{3+}) = 1.80 V$) are less reactive [17,106]. Therefore, the decomposition of H_2O_2 into $HO^·$ rather than $O_2^{·-}$, O_2, and H_2O is the most effective reaction pathway for H_2O_2, and how to achieve the efficient decomposition of H_2O_2 is still worth exploring.

In addition to the above two controversial topics, how to improve heterogeneous Fenton catalytic efficiency is the most concerned issue. In the heterogeneous Fenton system, the production of $HO^·$ via the reaction between Fe(II) and H_2O_2 is the most efficient and essential step for the removal of contaminants. Thus, some strategies that can accelerate the regeneration of Fe(II), promote the decomposition of H_2O_2, and in situ generate H_2O_2 may significantly enhance the heterogeneous Fenton reactivity. Based on these theoretical directions, many researchers have carried out a variety of related studies, such as introducing additional electrons (e.g., from external electric fields, electron-rich materials, semiconductors, plasmonic materials, or doped metals) to accelerate the generation of Fe(II) [30,31,36,37,42,43,63,76,86,116,133,137,171]; controlling the morphologies and exposed facets of catalysts to promote the decomposition of H_2O_2 [39,41,92,142,157–164]; and combining with ultrasound, electricity, semiconductors, and iron-based catalysts in the system to in situ generate H_2O_2 [7,56,99,153–156,172–175]. In addition, we briefly introduced some recent heterogeneous Fenton-like reactions which are of particular interest, including constructing dual reaction centers (i.e., the electron-poor center and the electron-rich center) [166–168] and synthesizing single-atom catalysts [169,170] to enhance the heterogeneous Fenton-like reactivity. The advantages of these strategies are summarized in Table 3, together, these approaches have significantly promoted the efficiency and advanced the applicability of heterogeneous Fenton reaction systems, as will be introduced in detail below.

3. Physical field-assisted heterogeneous Fenton processes

Introducing external energy, such as UV–vis light, electricity, microwave radiation, and ultrasound, to enhance the heterogeneous Fenton process has attracted much attention [7,19]. Typical physical fields include photo fieldS, electric fieldS, microwave fieldS, and sono fieldS in heterogeneous Fenton processes; these correspond to the photo-assisted [24,27], electro-assisted [107,108], microwave-assisted [109,110], and sono-assisted [111,112] heterogeneous Fenton processes, respectively. These physical field-assisted heterogeneous Fenton processes have been well studied over the years. Therefore, in this review, we will only briefly introduce this section to keep this review comprehensive and concise; and more detailed information about this topic has been presented in other reviews [7,19,108].

The heterogeneous photo-Fenton reaction is a combination of Fenton reagents and UV–vis light that generates additional $HO^·$ via (i) photoreduction of ferric ions (which leach from iron complexes and exist in the form of $Fe(OH)^{2+}$ under acidic conditions) to ferrous ions (Eqs. 10 − 11) and (ii) hydrogen peroxide photolysis (Eq. 12); the reaction is fundamentally related to redox processes [3,4,7].

$$Fe^{3+} + H_2O \rightarrow Fe(OH)^{2+} + H^+ \tag{10}$$

$$Fe(OH)^{2+} + h\nu \rightarrow Fe^{2+} + HO^· \ (\lambda < 580 nm) \tag{11}$$

$$H_2O_2 + h\nu \rightarrow 2 HO^· \ (\lambda < 310 nm) \tag{12}$$

On the other hand, some iron-based heterogeneous Fenton catalysts are also semiconductors, which can be excited to produce photo-generated electrons and holes under the irradiation of light, resulting in a reaction between adsorbed contaminants and H_2O_2 to produce ROS (Eqs. 13 − 15) [27,63]. For example, hematite, with a narrow band gap of 2.2 eV, can absorb the light up to 560 nm and collect approximately 40% of solar spectrum energy, presenting a promising material for photo-Fenton catalytic applications [40,176]. The band gap, valence band, and conduction band of different iron-based catalysts are summarized in Table 4. Ruales-Lonfat et al. [177] found that after introducing simulated solar light, the photo-Fenton catalytic activities of hematite, goethite, wüstite, and magnetite were significantly enhanced.

$$\text{Iron-based catalysts} + h\nu \rightarrow e^- + h^+ \tag{13}$$

$$h^+ + RH \rightarrow R^· + H^+ \tag{14}$$
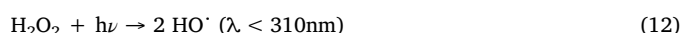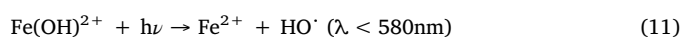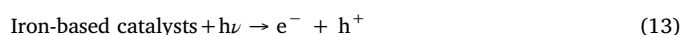
Table 3

Summary of strategies for enhancing heterogeneous Fenton/Fenton-like catalytic reactivity. The advantages of these strategies are listed below: ① accelerated redox cycling of Fe(III)/Fe(II); ② promoted H_2O_2 decomposition to generate ROS; ③ improved utilization efficiency of H_2O_2 by reducing the low-efficient decomposition of H_2O_2, ④ reduced H_2O_2 dosage; and ⑤ achieved maximum atom efficiency.

Strategies	Classification	Examples	Advantages	References
Introducing physical field	UV-Vis light	Photo-Fenton	①②	[24,27]
	Electricity	Electro-Fenton	①②④	[107,108]
	Microwave	Microwave-Fenton	①②	[109,110]
	Ultrasound	Sono-Fenton	①②④	[111,112]
Combining with electron-rich materials	NZVI	NZVI	①②	[32,33,77,113,114,115,116]
	Carboxylates	EDTA, oxalate, citrate	①②	[37,86,103,117,118,119,120,121,122]
	Carbon materials	CNTs, GO, biochar	①②	[22,30,35,81,95,123,124,125,126,127,128,129,130]
	Metal sulfides	MoS_2, WS_2, Cr_2S_3, CoS_2	①②	[28,131,132]
	Other reducing species	HA, sodium thiosulfate	①②	[45,133,134,135,136,137,138,139,140,141,142,143,144]
Introducing photo-generated electrons from photosensitive materials	Semiconductors	TiO_2, Ag_3PO_4, $BiVO_4$	①②	[16,31,63,67,68,82,145,146,147]
	Plasmonic catalysis	Ag/AgX (X = Cl, Br)	①②③	[11,42,51,72,148]
Introducing doped metals	/	Co, Mn, Cu, Cr, Ti, Zn	①②	[3,32,33,43,149,150,151,152]
In situ generation of H_2O_2	/	TiO_2, C_3N_4, pyrite	④	[99,153,154,155,156]
Facet and morphology control of catalysts	/	Hematite, magnetite	②	[39,41,92,142,157,158,159,160,161,162,163,164]
Novel heterogeneous Fenton-like reactions	Dual reaction centers	γ-Cu − Al_2O_3, d-TiCuAl–SiO_2	③	[165,166,167,168]
	Single-atom catalysis	FeN_x/g-C_3N_4, CoN_4/graphene	⑤	[169,170]

Table 4
Band gap, valence band, and conduction band of iron-based catalysts.

Catalyst	Band gap (eV)	Valence band (eV)	Conduction band (eV)	References
Magnetite	0.10	0.27	0.17	[178,179]
Hematite	2.20	2.41	0.21	[179,180]
Goethite	2.50	2.42	0.21	[181]
Akaganèite	2.06	/	/	[50]
Lepidocrocite	2.40	2.60	0.20	[182]
Maghemite	2.30	2.59	0.29	[179]
Pyrite	0.95	1.15	0.20	[178,183]
Pseudobrookite	1.95	/	/	[184]
$CoFe_2O_4$	1.33	1.33	1.33	[98]
FeOCl	1.85	1.95	0.10	[185]
$BiFeO_3$	1.61	/	/	[82]
$ZnFe_2O_4$	1.92	/	/	[186]
$MnFe_2O_4$	1.61	/	/	[187]
$LaFeO_3$	2.07	/	/	[188]
FeO	2.40	/	/	[178]
$FeTiO_3$	2.80	/	/	[178]
$YTiO_3$	2.60	/	/	[178]
$CuFeS_2$	0.35	/	/	[178]
Cu_5FeS_4	1.00	/	/	[178]
FeS	0.10	/	/	[178]
FeS_2	0.95	/	/	[178]
Fe_3S_4	0.00	/	/	[178]
FeAsS	0.20	/	/	[178]
$CdFe_2O_4$	2.30	/	/	[178]

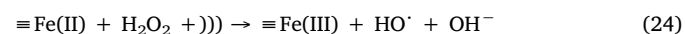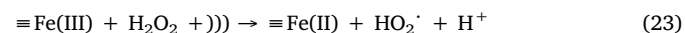$$e^- + H_2O_2 \rightarrow HO^· + OH^- \quad (15)$$
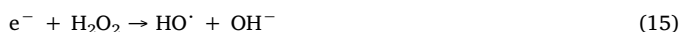
Electrochemical processes combined with heterogeneous Fenton processes can promote the degradation of organic contaminants [7,189,190]. In a heterogeneous electro-assisted Fenton process, H_2O_2 can be generated in situ via two-electron reduction of dioxygen on the cathode surface in acidic solution when an electrochemical process is applied (Eq. 16) [7]. In addition, the reduction of Fe^{3+}, which is leached from heterogeneous iron-based catalysts or directly supplied by sacrificing the corresponding Fe anode may occur simultaneously at the cathode (Eq. 17) [7]. Moreover, H_2O molecules may be oxidized into O_2 at the anode, increasing dissolved O_2 to generate more H_2O_2 (Eq. 18) and consequently promoting the generation of $HO^·$ [25]. In some high-oxygen overvoltage anodes, such as dimensionally stable anode, Pt, and boron-doped diamond anode, $HO^·$ can be generated on these anodes in the electro-Fenton reaction according to Eq. (19) [3,191]. For example, Nidheesh et al. 2014 [192] showed that magnetite exhibited high degradation efficiency towards Rhodamine B in an electro-Fenton reaction system, in which H_2O_2 was produced, while Fe^{3+} was reduced to Fe^{2+} at the cathode.

$$2e^- + 2H^+ + O_2 \rightarrow H_2O_2 \quad (16)$$

$$Fe^{3+} + e^- \rightarrow Fe^{2+} \quad (17)$$

$$H_2O \rightarrow 1/2O_2 + 2H^+ + 2e^- \quad (18)$$

$$H_2O \rightarrow HO^· + H^+ + e^- \quad (19)$$

Microwave radiation is a wavelength band of the electromagnetic spectrum with frequencies ranging from 300 MHz to 300 GHz, which can enhance heterogeneous Fenton processes via strong oxidation performance with short reaction times and high catalytic efficiency [110]. When microwaves are absorbed by heterogeneous Fenton catalysts, the dipoles align and flip around since the applied field is alternating, resulting in the formation of "hot spots" [193]. On one hand, these "hotspots" can induce the molecular rotation and then decrease the activation energy [193]. On the other hand, they can make heterogeneous Fenton catalysts more active in heterogeneous Fenton reactions and thus improve the effectiveness of the reaction [194]. Some studies pointed out that under the irradiation of microwave, the

heterogeneous Fenton reactivity can dramatically enhance and achieve the total degradation of contaminants within only a short time, and the catalysts can be reused several times without obvious iron leaching [7,110,194]. For example, Du et al. 2018 introduced microwave to the heterogeneous Fenton process for removing tri(2-chloroethyl)phosphate (TCEP) by iron ore tailing for the first time [195]. The degradation rate of TCEP in "microwave + H_2O_2 + iron ore tailing" system was 100% within 35 min, while only 12% TCEP was degraded in "H_2O_2 + iron ore tailing" system, which may be due to the high temperature and the production of extra $HO^·$ in microwave enhanced heterogeneous Fenton process.

Ultrasound waves are sound waves with a frequency greater than the upper limit of human hearing (approximately 20 kHz), which can create expansion and compression cycles to reduce pressure in liquids [19]. If the amplitude of the ultrasound pressure is large enough, ultrasound can result in acoustic cavitation, which is defined as the formation, growth, and subsequent collapse of microbubbles or cavities occurring in an extremely small interval of time (microseconds), releasing a large amount of energy at millions of such locations in the reactor [25]. When these bubbles explosively collapse, the pressure and temperature in the bubbles can reach up to several hundred atmospheres and several thousand Kelvin, respectively, which are beneficial for degradation in heterogeneous catalytic systems [19]. Under these conditions, ultrasonication can dissociate H_2O and O_2 to generate $HO^·$ and H_2O_2 (Eqs. (20)–(22), ")))" represents ultrasound waves) [19,196]. In addition, Khataee et al. 2016 [196] pointed out that ultrasonic waves can promote the redox cycling of Fe(III)/Fe(II) (Eqs. 23,24) and, therefore, significantly enhanced the degradation of Reactive Blue 69 in an ultrasonic/H_2O_2/pyrite system.

$$H_2O +))) \rightarrow H^· + HO^· \quad (20)$$

$$O_2 +))) + 2H_2O \rightarrow 4HO^· \quad (21)$$

$$4H^· + 2O_2 \rightarrow 2H_2O_2 \quad (22)$$

$$\equiv Fe(III) + H_2O_2 +))) \rightarrow \equiv Fe(II) + HO_2^· + H^+ \quad (23)$$

$$\equiv Fe(II) + H_2O_2 +))) \rightarrow \equiv Fe(III) + HO^· + OH^- \quad (24)$$

Interestingly, combining heterogeneous Fenton reactions with two kinds of physical fields can further promote the reactivity of catalysts, such as in the sono-photo-Fenton process, sono-electro-Fenton process, photo-electro-Fenton process, and microwave-photo-Fenton process [7,19]. For example, microwave irradiation can not only enhance the photocatalytic activity via suppressing the recombination of electron-hole pairs [197] but also accelerate the reduction of Fe(III) to Fe(II) in the electro-Fenton reaction system [198]. Wang et al. 2012 [198] demonstrated that under microwave irradiation, both cathode and anode surfaces were activated efficiently in the electro-Fenton oxidation process. As shown in Fig. 2, microwave irradiation can not only accelerate the Fe(III)/Fe(II) redox cycles but also facilitate the electro-synthesis of H_2O_2 from O_2 on the cathode via promoting the transduction of electrons.

4. Combining heterogeneous Fenton catalysts with electron-rich materials

As discussed above, the low generation speed of Fe(II) is the rate-limit step in the heterogeneous Fenton reaction. Therefore, in recent years, large numbers of studies have focused on directly combining electron-rich materials with heterogeneous Fenton catalysts, and electrons from these materials can accelerate the generation of Fe(II), resulting in high heterogeneous Fenton reactivity. Usually, these electrons can be directly provided from nZVI [76,116], carboxylates [37,86], carbon materials [30,171], metal sulfides [28,131,132], and other reducing species [133,137].
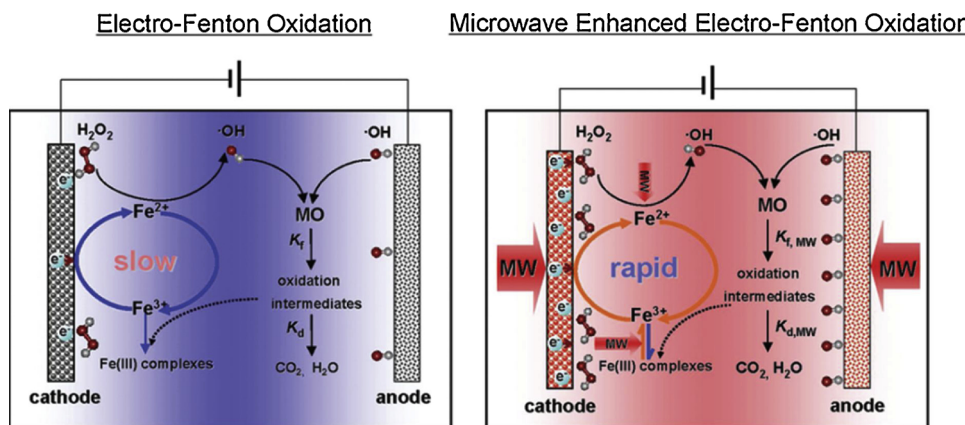
Electro-Fenton Oxidation   Microwave Enhanced Electro-Fenton Oxidation

Fig. 2. Possible mechanism of a microwave-enhanced electro-Fenton oxidation reaction; microwave irradiation can accelerate the redox cycles of Fe(III)/Fe(II) and the decomposition of H_2O_2. Reproduced from Ref. [198], Copyright (2012), with permission from American Chemistry Society.

4.1. Directly injecting electrons from nZVI

nZVI (Fe^0) has been studied as a low-cost and innocuous reductant ($E^0 = -0.44$ V) in environmental remediation processes to remove various organic and inorganic contaminants [74,199]. In general, contaminant removal by nZVI is achieved by the direct transfer of electrons from nZVI to the contaminants, reducing the contaminants into less toxic or non-toxic species [199].

Some attempts have also proposed to replace Fe^{2+} with Fe^0 to participate in the Fenton reaction [200,201], in which nZVI can be oxidized to Fe^{2+} both by H_2O_2 and molecular oxygen (O_2) in acidic conditions (Eqs. 5,6) [200,201], which would further promote the generation of $HO^·$ (Eq. 1). However, extra H_2O_2 is needed to produce Fe^{2+} in the acidic system of Fe^0/H^+ (Eq. 25), resulting in low H_2O_2 utilization efficiency. In addition, Joo et al. [202] pointed out that only 7% of nZVI can be oxidized to Fe^{2+} at neutral pH in the nZVI/O_2 system, which restricts the application of nZVI in the Fenton reaction.

In recent years, some studies have focused on combining nZVI with iron oxides in the heterogeneous Fenton reaction by using the excellent reducing properties of Fe^0 to achieve a high Fe(III)/Fe(II) redox cycling rate (Eq. 7), by which the electrons from Fe^0 can be used effectively [76,203]. Zhang and his group synthesized a series of Fe@Fe$_2$O$_3$-based core-shell nanocatalysts, such as Fe@Fe$_2$O$_3$ [77,113–116], ascorbic acid/Fe@Fe$_2$O$_3$ [140], Fe(II)/Fe@Fe$_2$O$_3$ [204,205], and tetrapolyphosphate/Fe@Fe$_2$O$_3$ [203], to accelerate the Fe(III)/Fe(II) redox cycle, and the mechanisms in these systems were analyzed in detail. For example, in the Fe@Fe$_2$O$_3$ system [116], two electrons from Fe^0 can transfer to O_2 to generate H_2O_2 (Eq. 6), which further reacts with generated Fe^{2+} to produce $HO^·$ under acidic to neutral pH conditions (Eq. 1) (Fig. 3). In addition, Fe@Fe$_2$O$_3$ can activate molecular oxygen to produce $O_2^{·−}$ via the single-electron reduction pathway (Eqs. 26 − 28).

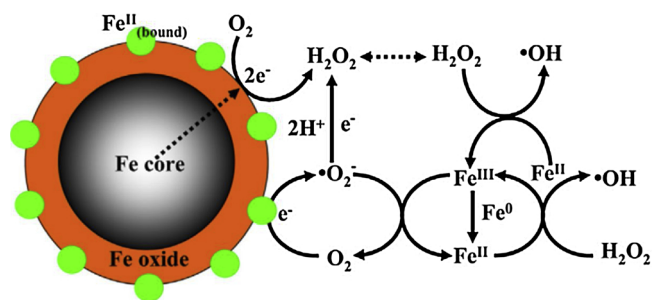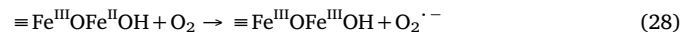**Fig. 3.** Schematic illustration of enhanced Fenton oxidation by Fe@Fe$_2$O$_3$ nanowires at pH > 4; two electrons from Fe^0 reduce O_2 to generate H_2O_2, promoting the production of $HO^·$. Reproduced from Ref. [116], Copyright (2014), with permission from Elsevier.

These $O_2^{·−}$ together with Fe^0 can accelerate Fe^{3+}/Fe^{2+} cycles to guarantee a steady supply of Fe^{2+} for H_2O_2 decomposition to produce more $HO^·$ (Eqs. 25 and 29).

$$Fe^0 + 2Fe(III) \rightarrow Fe(II) \tag{25}$$

$$\equiv Fe^{III}OH + Fe^{2+} + H_2O \rightarrow \equiv Fe^{III}OFe^{II}OH + 2H^+ \tag{26}$$

$$\equiv Fe^{III}OFe^{II}OH \rightarrow \equiv Fe^{II}OFe^{III}OH \tag{27}$$

$$\equiv Fe^{III}OFe^{II}OH + O_2 \rightarrow \equiv Fe^{III}OFe^{III}OH + O_2^{·−} \tag{28}$$

$$O_2^{·−} + Fe(III) \rightarrow Fe(II) + O_2 \tag{29}$$

4.2. Directly injecting electrons from carboxylates

Carboxylates are a kind of chelating agent that contains carboxyl groups, and their immobilization on different supporting materials for water treatment has received wide attention due to their merits of non-volatile, cheap, and non-toxic nature [118]. Many carboxylates are naturally occurring organic acids, such as oxalate, citrate, humic acids, and tartrate, which have a widespread distribution in nature [121]. These carboxylates can form strong complexes with Fe(III) due to the ligand-to-metal charge transfer process; the complexes are usually very stable below neutral pH [206]. In addition, several studies found that some carboxylates (e.g., ascorbic acid and humic acids) are antioxidants that can accelerate Fe(III)/Fe(II) cycling to enhance contaminant degradation in the Fenton system [77,137,140,142,207].

In recent years, a number of studies have focused on studying the effect of different carboxylates on the heterogeneous Fenton reaction, and the results showed that carboxylates can significantly promote the degradation of contaminants [77,140,142]. For example, Hou et al. [140] combined ascorbic acid and Fe@Fe$_2$O$_3$ core-shell nanowires (AA/Fe@Fe$_2$O$_3$), and found that the contaminant degradation constants in the AA/Fe@Fe$_2$O$_3$/H_2O_2 Fenton systems were 38–53 times higher than those in the conventional homogeneous Fenton system (Fe(II)/H_2O_2) at pH 3.8. They deduced that during the AA/Fe@Fe$_2$O$_3$/H_2O_2 Fenton process, ascorbic acid served as a reducing and complexing reagent, promoting the Fe(III)/Fe(II) redox cycle, as shown in Fig. 4.

On the other hand, many studies have demonstrated that the photochemical dissociation of Fe(III)-carboxylate complexes in aqueous solution involved the reduction of Fe(III) to Fe(II) and concomitant oxidation of carboxylic acid [206,208,209]. For example, Abida et al. 2012 [206] noted that Fe(III)–citrate complexes (Fe(III)–Cit) can generate Fe(II) and $R-CO_2^·$ by the redox process between Fe(III) and the carboxylate group under the irradiation of UV light (Eq. 30). After that, fast decarboxylation of the citrate radical is probably obtained, and ROS such as $HO_2^·/O_2^{·−}$, H_2O_2, and $HO^·$ are generated afterward
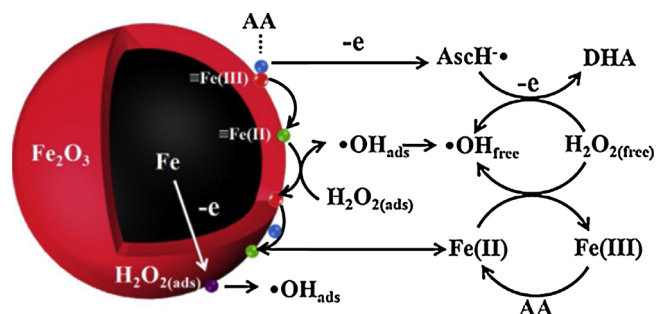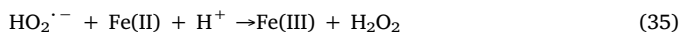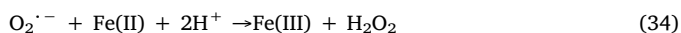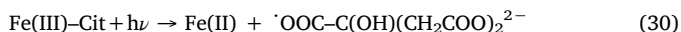
Fig. 4. Schematic illustration of the reaction mechanism in the AA/Fe@Fe$_2$O$_3$/H$_2$O$_2$ system; ascorbic acid served as a reducing and complexing reagent to promote the Fe(III)/Fe(II) redox cycle on Fe$_2$O$_3$. Reproduced from Ref. [140], Copyright (2016), with permission from Elsevier.

according to Eqs. 4 and 31–35.

$$Fe(III)-Cit + h\nu \rightarrow Fe(II) + \cdot OOC-C(OH)(CH_2COO)_2^{2-} \tag{30}$$

$$\cdot OOC-C(OH)(CH_2COO)_2^{2-} \rightarrow \cdot C(OH)(CH_2COO)_2^{2-} + CO_2 \tag{31}$$

$$\cdot C(OH)(CH_2COO)_2^{2-} + O_2 \rightarrow OC(CH_2COO)_2^{2-} + HO_2\cdot \tag{32}$$

$$HO_2\cdot \rightarrow O_2^{\cdot-} + H^+ \tag{33}$$

$$O_2^{\cdot-} + Fe(II) + 2H^+ \rightarrow Fe(III) + H_2O_2 \tag{34}$$

$$HO_2^{\cdot-} + Fe(II) + H^+ \rightarrow Fe(III) + H_2O_2 \tag{35}$$

In addition, other studies have pointed out that the complexation of Fe^{3+}/Fe^{2+} with carboxylates decrease the Fe^{3+}/Fe^{2+} redox potential from 0.77 to 0.356, 0.256, and 0.209 V (vs. NHE) for disodium nitrilotriacetate, oxalate, and EDTA, respectively, promoting the decomposition rate of H$_2$O$_2$ [86,122]. Wang et al. 2011 [86] studied the effects of chelating agents on the catalytic degradation of BPA in the H$_2$O$_2$/BiFeO$_3$ heterogeneous Fenton system, and they found that BPA degradation was considerably accelerated in the pH range of 5–9 after adding proper organic ligands. In addition, the enhancing effect of these ligands followed the order blank < tartaric acid < formic acid < glycine < nitrilotriacetic acid < EDTA. In the presence of ligands, the strong complexing ability makes the chelating agents easily adsorbed on surface $\equiv$Fe^{3+} sites. Thermodynamically, the standard redox potential of Fe^{3+}-EDTA/Fe^{2+}-EDTA (0.17 V) is lower than that of Fe^{3+}/Fe^{2+} (0.77 V), which makes the oxidation of Fe^{2+}-EDTA by H$_2$O$_2$ more favorable.

4.3. Directly injecting electrons from carbon materials

Carbon materials, such as polyhydroxy fullerene (PHF) [35], hydrothermal carbon (HTC) [123], activated carbon (AC) [22,124], carbon nanotubes (CNTs) [125,126], graphene oxides (GO) [30,95], biochar [127,128], g-C$_3$N$_4$ [81,129], and porous carbon [130], have been widely applied in heterogeneous Fenton reactions because of their abundant electrons and ubiquitous existence in natural environments [171]. During the last two decades, numerous studies have reported the excellent ability of carbon materials to activate various oxidants, such as H$_2$O$_2$, O$_2$, and persulfate (including peroxymonosulfate and peroxodisulfate), to form ROS for the degradation of refractory organic contaminants [35,171,210,211]. For example, Zhou and her group found that biochars (produced from pine needles, wheat, and maize straw) can activate O$_2$, H$_2$O$_2$, and persulfate through a direct single-electron transfer process to generate reactive free radicals for the degradation of organic contaminants [127,128,212]. Moreover, Kurniawan and Lo [210] pointed out that AC can be regarded as an electron-transfer catalyst, similar to the Haber–Weiss mechanism involving the reduced (AC) and oxidized (AC$^+$) catalyst states to produce HO$\cdot$ and HO$_2\cdot$ (Eqs. 36–37). Since then, other carbon materials, such as GO and CNTs, have also been proven to undergo a similar mechanism and can significantly enhance the heterogeneous Fenton reaction [30,126].

$$AC + H_2O_2 \rightarrow AC^+ + HO\cdot + OH^- \tag{36}$$

$$AC^+ + H_2O_2 \rightarrow AC + HO_2\cdot + H^+ \tag{37}$$
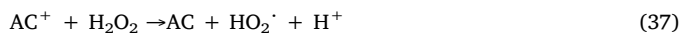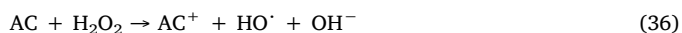
On the other hand, many researchers have noted that combining carbon materials with a heterogeneous Fenton catalyst can improve the Fenton reactivity dramatically because of the strong ability of electron transfer to accelerate the reduction of Fe(III) to Fe(II) [30,35,126]. Xu et al. [35] found that, under simulated sunlight irradiation, the photo-Fenton activity in the degradation of acid red 18 by PHF modified ferrihydrite was enhanced compared with that obtained by pure ferrihydrite. They pointed out that the excited-state PHF can efficiently sensitize the ground-state O$_2$ to generate ^{1}O$_2$ and at the same time can transfer electrons to ferrihydrite, accelerating the reduction of Fe(III) to Fe(II). In addition, Qin et al. 2017 [123] synthesized HTC via a hydrothermal process with different procedures (e.g., D-glucose, sucrose, fructose, or starch), and they found that HTC favored alachlor degradation in the Fe(III)/H$_2$O$_2$ system by promoting Fe(III)/Fe(II) cycling via electron transfer from HTC to Fe(III).

Zubir et al. [30] synthesized a GO–Fe$_3$O$_4$ composite by co-precipitating pre-hydrolyzed ferric and ferrous salts in the presence of GO. The GO–Fe$_3$O$_4$ composite presented much higher reactivity and stability than pure Fe$_3$O$_4$ towards the degradation of acid orange 7. Fig. 5A
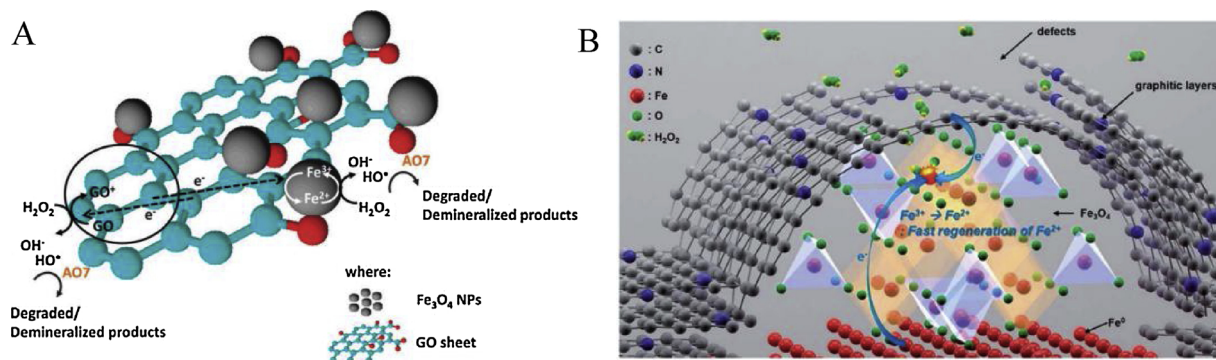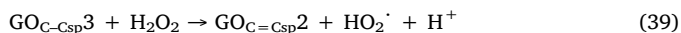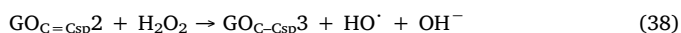

Fig. 5. (A) Proposed mechanism for GO–Fe$_3$O$_4$ activity in the heterogeneous Fenton reaction; the unpaired π electrons of GO can be transferred between the GO and iron centers to accelerate the reduction of Fe^{3+} to Fe^{2+}. Reproduced with permission from ref.[29], Copyright 2015, The Royal Society of Chemistry; (B) Suggested mechanism in the Fe$_3$O$_4$/Fe/Fe$_3$C@PCNF system; Fe^0 and the delocalized π electrons of the graphitic layers accelerate the redox cycling of Fe^{3+}/Fe^{2+}, and the defects from the defective graphitic layers promote the H$_2$O$_2$ decomposition around carbon and Fe$_3$O$_4$. Reproduced from Ref. [130], Copyright (2017), with permission from The Royal Society of Chemistry.

displays the proposed mechanism related to the synergistic interfacial effect of the GO sheet and Fe_3O_4. GO can be regarded as an electron-transfer catalyst, similar to the Haber–Weiss mechanism involving the reduced and oxidized catalyst states to compose H_2O_2 to $HO^{\cdot}$ and $HO_2^{\cdot}$ (Eqs. 38–39). On the other hand, the unpaired π electrons of GO can be transferred between the GO and iron centers to accelerate the reduction of Fe^{3+} to Fe^{2+}. In the whole reaction processes, GO plays a sacrificial role via the oxidation of C=C carbon domains, transferring electrons to Fe_3O_4, resulting in superior catalytic efficiency and recyclability.

$$GO_{C=Csp}2 + H_2O_2 \rightarrow GO_{C-Csp}3 + HO^{\cdot} + OH^{-} \tag{38}$$

$$GO_{C-Csp}3 + H_2O_2 \rightarrow GO_{C=Csp}2 + HO_2^{\cdot} + H^{+} \tag{39}$$

Yoo et al. [130] synthesized a heterogeneous Fenton catalyst exhibiting extremely high H_2O_2 decomposition rate based on $Fe_3O_4/Fe/$ cementite(Fe_3C) nanoparticles supported on porous carbon nanofiber (PCNF), namely $Fe_3O_4/Fe/Fe_3C@PCNF$. The H_2O_2 decomposition rate (k_{obsd}) was estimated as $0.8398\,min^{-1}\,(g\,L^{-1})^{-1}$ ($7.776\,M^{-1}\,s^{-1}$, calculated by thermogravimetric analysis), which is the highest value ever reported. In addition, this material showed a high removal activity of aqueous methylene blue tested under various conditions. The possible mechanism for the high H_2O_2 decomposition rate and high methylene blue removal rate was proposed, as shown in Fig. 5B: (1) Fe^0 and delocalized π-electrons of graphitic layers accelerate the redox cycle of Fe^{3+}/Fe^{2+}; (2) the defects from the defective graphitic layers of catalyst particles promote H_2O_2 decomposition; (3) the defective graphitic layers can partially cover the catalyst, resulting in the decomposition reaction around carbon and Fe_3O_4.

Yang et al. 2018 [125] noted that in the Fe(III)-mediated functionalized multi-walled CNTs (FCNT-H-Fe(III)) system, a new pathway was revealed: in addition to a small fraction of Fe(III) being reduced by FCNT-H, 80% of Fe(III) was reduced by H_2O_2. Deng et al. [73] used biochar-supported nZVI as an activator for the Fenton removal of sulfamethazine (SMT). nZVI can decompose H_2O_2 to generate $HO^{\cdot}$ for the degradation of SMT, while biochar played multiple roles, i.e., preventing nZVI aggregation, adsorbing SMT, activating H_2O_2, and alleviating nZVI passivation. Yan et al. [213] proposed that in the nZVI/ biochar composite, the C−OH bound on biochar can activate H_2O_2 to generate $HO^{\cdot}$ through a single-electron transfer process (Eq. 40).

$$C-OH + H_2O_2 \rightarrow HO^{\cdot} + CO^{\cdot} + H_2O \tag{40}$$
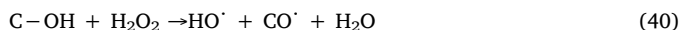
4.4. Directly injecting electrons from metal sulfides

Most recently, some studies found that metal sulfides (MoS_2, WS_2, Cr_2S_3, CoS_2, PbS, or ZnS) can serve as excellent co-catalysts to accelerate the rate-limiting step of Fe^{3+}/Fe^{2+} conversion by the exposed reductive metallic active sites [28,131,132]. For example, Xing et al. 2018 [28] combined Fe^{3+} with various metal sulfides, such as MoS_2, WS_2, Cr_2S_3, CoS_2, PbS, and ZnS to compare the contributions of these metal sulfides to the Fenton reaction. They found that the efficiency of reduction of Fe^{3+} to Fe^{2+} followed the order: $WS_2 > CoS_2 > ZnS > MoS_2 > PbS > Cr_2S_3 >$ conventional Fenton. Specifically, the reaction rate constant (K_a) value for the degradation of Rhodamine B by the $FeSO_4 + MoS_2 + H_2O_2$ mixture was 18.5 times than that of the $FeSO_4 + H_2O_2$ system. In addition, even the optimal activity of the $FeSO_4 + H_2O_2$ system ($H_2O_2 = 1.0\,mmol/L$) was much lower than that of $FeSO_4 + MoS_2 + H_2O_2$ at a lower concentration of H_2O_2 (0.4 mmol/L). As shown in Fig. 6, the unsaturated S atoms on the surface of metal sulfides can capture protons to form H_2S. After the removal of S atoms, the exposed Mo^{4+} becomes very reactive, facilitating the reduction of Fe^{3+} to Fe^{2+} (Eq. 41). After that, Mo^{6+} can be converted back to Mo^{4+} by the reaction with H_2O_2 (Eq. 42), which ensures the catalytic cycling of MoS_2. In addition, the authors found that commercial MoO_3 has a similar co-catalytic effect in the degradation of Rhodamine B, but the activity was significantly lower than

that of MoS_2, mainly due to the lack of defects exposed on the surface of MoO_3.

$$Mo^{4+} + 2Fe^{3+} \rightarrow Mo^{6+} + 2Fe^{2+} \tag{41}$$

$$Mo^{6+} + H_2O_2 \rightarrow Mo^{4+} + 2H^{+} + O_2 \tag{42}$$
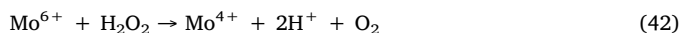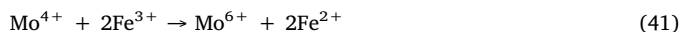
4.5. Directly injecting electrons from other reducing species

Some reducing species, such as hydroxylamine (HA), can reduce many electron acceptors, such as H_2O_2, Fe(III), and Cu(II) [135,144]. Moreover, Chen et al. [214] demonstrated that HA can decompose H_2O_2 to produce $HO^{\cdot}$ without transition metals because of its high reducibility. Considering the properties of these reducing species, many researchers have added HA, sodium thiosulfate, and sodium sulfite to the heterogeneous Fenton reaction to accelerate the redox cycle of Fe (III)/Fe(II) in recent years [45,133–144].

Wu et al. [134] added different reducing agents, i.e., HA, sodium thiosulfate, ascorbic acid, sodium ascorbate, and sodium sulfite, to the persulfate/Fe(II) system to accelerate the regeneration of Fe(II) and found HA was the most efficient species in trichloroethylene degradation. Hou et al. [45] constructed a surface Fenton system with HA, goethite, and $H_2O_2(\alpha$-FeOOH–HA/H_2O_2) to degrade various contaminants, and they found that HA can accelerate the Fe(III)/Fe(II) redox cycle, greatly promoting H_2O_2 decomposition on the α-FeOOH surface to produce $HO^{\cdot}$ without releasing any detectable iron ions during the Fenton reaction process. Additionally, Ma and his group published several papers about the positive effect of HA on the heterogeneous Fenton reaction [133–136,139], and they also demonstrated that HA can activate H_2O_2 to generate $HO^{\cdot}$ without a transition metal [135].

Although these reducing species can directly provide electrons to reduce Fe(III); multiple recycling of these species is difficult to achieve as the available electrons from the donor component on these materials are limited. In addition, some organic compounds (e.g., some carboxylates and HA) will eventually be degraded in the Fenton reaction, and they will consume part of the produced $HO^{\cdot}$ as well [135,215]. Moreover, the accumulation of ferric oxyhydroxides on the surface of nZVI in neutral to slightly alkaline environments will reduce the reactive surface area for the formation of hydroxyl radicals and hamper the electron supply from nZVI [19].

5. Introducing photo-generated electrons to heterogeneous Fenton catalysts

Considering that the available electrons from the above reducing species will gradually be exhausted as the reaction continues, some studies have focused on introducing photo-generated electrons to the heterogeneous Fenton reaction. These electrons from semiconductors (e.g., TiO_2, $BiVO_4$, and C_3N_4) and plasmonic catalysts (e.g., Ag/AgCl and Ag/AgBr) can be continuously injected into heterogeneous catalysts, which can accelerate the reduction of Fe(III) to Fe(II), leading to a high degradation efficiency of the target organic contaminants. In addition, with the reduction of Fe(III) by these electrons, the consumption of H_2O_2 for the production of $Fe^{2+}/Fe(II)$ (Eqs. 2–3) can be minimized, resulting in much higher utilization efficiency of H_2O_2 [36].

5.1. Electrons from semiconductors

Recently, some studies have combined semiconductor materials (e.g., TiO_2, Ag_3PO_4, $BiVO_4$, CdS, and g-C_3N_4) with heterogeneous Fenton catalysts to enhance the Fenton catalytic activity due to the continuous generation of electrons by semiconductors [16,31,63,67,68,82,145–147]. Under light irradiation, electrons can be excited from the valence band of semiconductors to the conduction band (Eq. 43). As the potentials of these photo-generated electrons are
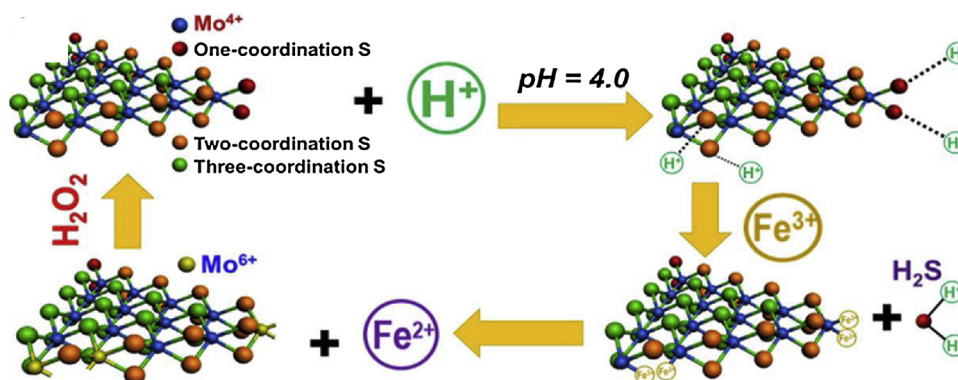
Fig. 6. Schematic illustration of the co-catalytic mechanism of MoS_2 in AOPs; exposed Mo^{4+} on the surface of MoS_2 facilitates the reduction of Fe^{3+} to Fe^{2+}. Reproduced from Ref. [28], Copyright (2017), with permission from The Royal Society of Chemistry.
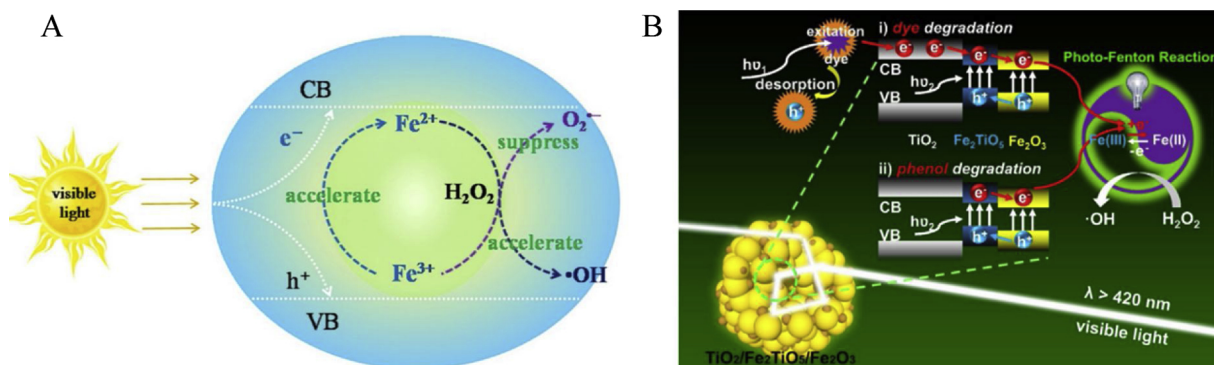

Fig. 7. (A) Possible photo-Fenton catalytic mechanism of $BiVO_4$/ferrihydrite. Reproduced from Ref. [16], Copyright (2017), with permission from Elsevier; (B) Visible-light-driven photo-Fenton reaction mechanism of $TiO_2/Fe_2TiO_5/Fe_2O_3$ for the removal of different organic pollutants. Reproduced from Ref. [63], Copyright (2017), with permission from Elsevier. The electrons from $BiVO_4$, Fe_2O_3, and TiO_2 can reduce Fe(III) to Fe(II), promoting the decomposition of H_2O_2.

lower than the redox potential of aqueous Fe^{3+}/Fe^{2+} (E_0 (Fe^{3+}/Fe^{2+}) = + 0.77 V vs. NHE) [16,216], aqueous Fe^{3+} can be continuously reduced to Fe^{2+} by these electrons, resulting in the enhancement of the homogeneous Fenton reactions (Eq. 44). On the other hand, Fe^{3+} can act as an electron acceptor to inhibit the recombination of photo-generated electron-hole pairs. Although the specific redox potential of solid Fe(III)/Fe(II) in these heterogeneous Fenton catalysts is uncertain, our group detected the generated Fe(II) during the heterogeneous photo-Fenton reaction by completely dissolving the catalysts to measure the concentration of Fe^{2+} in aqueous solution, indicating that the photo-generated electrons can also reduce solid Fe(III) to Fe(II) (Eq. 45) [11,16,36]. For example, Xu et al. [16] explored the photo-Fenton catalytic mechanism of a ferrihydrite-modified $BiVO_4$ ($BiVO_4$/Fh) composite by studying H_2O_2 decomposition, Fe(II) generation, and ROS formation at near-neutral pH. The results verified that the introduction of $BiVO_4$ to ferrihydrite can enhance H_2O_2 consumption and Fe(II) regeneration by the photo-generated electrons from $BiVO_4$ (Fig. 7A). The results further proved that enhanced H_2O_2 consumption was due to accelerated Fe(III) reduction by accepting photo-generated electrons from $BiVO_4$ rather than by direct consumption of H_2O_2 by $BiVO_4$. In addition, they noted that the introduction of $BiVO_4$ can enhance the photo-Fenton catalytic activity of Fh both at acidic and near-neutral pHs, and $BiVO_4$/Fh show high Fenton catalytic activity at near-neutral pH.

$$Semiconductors + h\nu \rightarrow e^- + h^+ \tag{43}$$

$$Fe^{3+} + e^- \rightarrow Fe^{2+} \tag{44}$$

$$Fe(III) + e^- \rightarrow Fe(II) \tag{45}$$

Wang and his group [31,147] synthesized yolk-shell (Y-S)

structured Fe_3O_4@void@CdS and Fe_3O_4@void@TiO_2 nanoparticles through a modified chemical bath deposition method. The Y-S structure can not only act as a nanoreactor to enrich the pollutant and provide a suitable reaction site but also maximize the use of light irradiation owing to light reflection in the hollow area. The photo-generated electrons from CdS and TiO_2 may transfer to the Fe_3O_4 cores to reduce Fe^{3+}, promoting the formation of HO˙. The authors also found that when the shell component changes to CeO_2, enhanced degradation efficiency can be achieved, indicating a general strategy of adding outer semiconductor shells to Fe_3O_4 cores.

As discussed in Section 3, some iron-based materials, such as Fe_2O_3 and FeOCl [40,63,180,185,217], can be excited to generate electron-hole pairs under light irradiation. The electrons in the conduction band of these iron-based materials can be self-generated and transferred from the conduction band of other semiconductors can participate in the conversion of Fe(III) to Fe(II). For example, Deng et al. [63] successfully synthesized a novel $TiO_2/Fe_2TiO_5/Fe_2O_3$ triple-heterojunction composite via facile ion-exchange combined with calcination. Fe_2TiO_5 was located at the interface between TiO_2 and Fe_2O_3, acting as a "bridge" to transfer the photo-excited electrons from TiO_2 to Fe_2O_3 (Fig. 7B). The excellent charge separation improved the lifetime of electrons and could reduce Fe(III) to Fe(II) on the surface of the heterojunction.
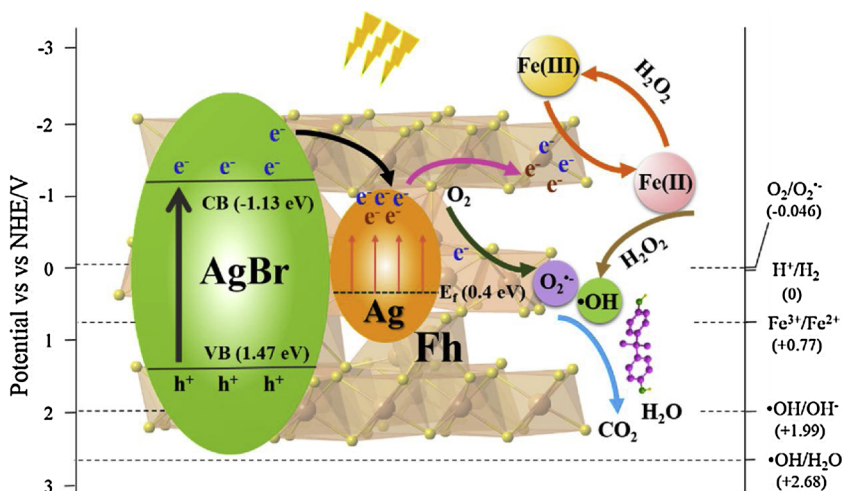
5.2. Electrons from plasmonic catalysts

In recent years, Ag nanoparticles and Ag/AgX (X=Cl and Br) catalysts have become a focus of research in the field of photo-Fenton reactions because they can strongly absorb visible light due to the surface plasmon resonance effect of Ag nanoparticles, the semiconductor properties of AgX, and the excellent electron transfer between Ag nanoparticles and AgX [11,42,51,72,148].

Chen et al. 2016 [42] synthesized Ag nanoparticle-modified cocoon-like hematite mesocrystal superstructure composites through a facile template-free approach in a benzyl alcohol solvent. Under visible light irradiation, the loaded Ag nanoparticles promoted the separation of charge carriers on hematite, resulting in excellent photo-Fenton performance in the degradation of Rhodamine B, methyl orange, and colorless glyphosate. In composites of Ag-SiO$_2$@α-Fe$_2$O$_3$ [148] and g-C$_3$N$_4$/Ag/γ-FeOOH [51], Ag nanoparticles perfectly act as centers for photo-generated electron transfer from semiconductors to iron catalysts to achieve Fe(III)/Fe(II) cycling under visible light. In addition, Liu et al. [72] synthesized a Ag/AgCl/Fe-sepiolite plasmonic photo-Fenton catalyst by ion-exchange and photo-reduction methods and found that Ag/AgCl/Fe-sepiolite exhibited excellent activity and stability for the degradation of BPA under visible light illumination.
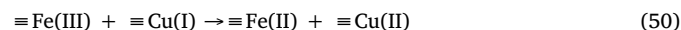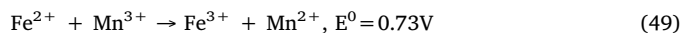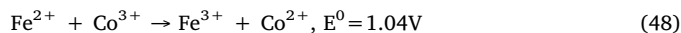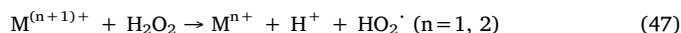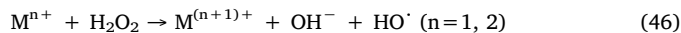
Our group further studied the effects of Ag/AgCl and Ag/AgBr on the ferrihydrite-based heterogeneous photo-Fenton reaction [11,36]. The degradation rate of BPA increases significantly after loading Ag/AgCl and Ag/AgBr on the surface of ferrihydrite. In addition, we detected generated Fe(II) in both of these two systems, indicating that Ag/AgCl and Ag/AgBr can accelerate Fe(III)/Fe(II) conversion by the photo-generated electrons. In the Ag/AgCl/ferrihydrite system, AgCl cannot absorb visible light because of the wide band gap of 3.25 eV. Therefore, the photo-generated electrons are all from the Ag nanoparticles, while AgCl acts as a center for electron transfer from the Ag nanoparticles to ferrihydrite. However, in the Ag/AgBr/ferrihydrite system, AgBr can be stimulated under visible light due to its narrow band gap of 2.6 eV. The generated Fe(II) in these samples and the degradation rate constants of BPA followed the same order: Ag/AgBr/ferrihydrite > AgBr/ferrihydrite > ferrihydrite, which can be attributed to the accelerated reduction of Fe(III) to Fe(II) by the photo-generated electrons from AgBr and Ag nanoparticles; furthermore, the system profited from the strong electron trapping ability of Ag nanoparticles in separating the electron-hole pairs of AgBr (Fig. 8). Moreover, we found that the reduction of Fe^{2+}/Fe(III) by the photo-generated electrons can reduce the decomposition of H$_2$O$_2$ for the regeneration of Fe^{2+}/Fe(II) (Eqs. 2–3), increasing the utilization efficiency of H$_2$O$_2$. In addition, both Ag/AgCl/ferrihydrite and Ag/AgBr/ferrihydrite composites exhibited relatively high heterogeneous Fenton reactivities at near-neutral pH. As such, direct solid phase reduction of Fe(III) by injection of photo-generated electrons can enhance the structural stability of the heterogeneous catalysts and reduce the effect of the increased solution pH.

6. Introducing doped metals in heterogeneous Fenton catalysts

Recently, many studies have shown that introducing doped metals, (e.g., Co, Mn, Cu, Cr, Ti, Zn, and Nb) to the structure of iron minerals (e.g., magnetite, hematite, and goethite) can significantly promote the Fenton reactivity [3,32,33,43,149–152]. Some polyvalent metals (e.g., Co, Mn, and Cu) can react with H$_2$O$_2$ to generate HO$_2$· and HO· via a Haber–Weiss-like mechanism during the Fenton reaction (Eqs. 46,47), which promote the decomposition of H$_2$O$_2$ [32,43]. In addition, these metals can participate in the redox cycling of Fe(III)/Fe(II) (Eqs. 48–50) [32,43].

$$M^{n+} + H_2O_2 \rightarrow M^{(n+1)+} + OH^- + HO^· \ (n=1, 2) \tag{46}$$

$$M^{(n+1)+} + H_2O_2 \rightarrow M^{n+} + H^+ + HO_2^· \ (n=1, 2) \tag{47}$$

$$Fe^{2+} + Co^{3+} \rightarrow Fe^{3+} + Co^{2+}, \ E^0 = 1.04V \tag{48}$$

$$Fe^{2+} + Mn^{3+} \rightarrow Fe^{3+} + Mn^{2+}, \ E^0 = 0.73V \tag{49}$$

$$\equiv Fe(III) + \ \equiv Cu(I) \rightarrow \equiv Fe(II) + \ \equiv Cu(II) \tag{50}$$

Costa and his coworkers [32] studied the effect of Co and Mn, in the structure of magnetite on heterogeneous Fenton reactions. They found that the incorporation of Co or Mn in the magnetite structure remarkably enhanced the Fenton reactivity of magnetite due to the increased decomposition of H$_2$O$_2$. On the other hand, the redox potential of Fe^{3+}/Fe^{2+} is 0.77 V, which is much lower than those of Co^{3+}/Co^{2+} (1.81 V) and Mn^{3+}/Mn^{2+} (1.51 V). Therefore, the reduction of Co^{3+} or Mn^{3+} by Fe^{2+} is thermodynamically favorable, as shown in Eqs. 48,49. Xu et al. [43] found that Cu-doped α-FeOOH presented higher photo-Fenton catalytic activity than pure α-FeOOH under visible light irradiation, which was attributed to the fact that Cu(I) can not only activate H$_2$O$_2$ via a Fenton-like reaction but also reduce Fe(III) to Fe(II). Nguyen et al. [33] synthesized Zn-doped Fe$_3$O$_4$ hollow submicrospheres (HSMSs) via a simple one-pot solvothermal route, during which Zn-rich amorphous shells first grew on the surfaces, and then Zn gradually diffused into the Fe$_3$O$_4$ crystals to form Zn-doped Fe$_3$O$_4$ due to the Kirkendall effect. The Zn-doped Fe$_3$O$_4$ HSMSs exhibited high and stable photo-Fenton activity for the degradation of Rhodamine B and cephalexin under visible light irradiation due to the accelerated electron transfer process between Fe(III) and H$_2$O$_2$ by doped Zn in the hollow mesocrystal structure.

7. Controlling the morphology and facets of heterogeneous Fenton catalysts

Over the past decade, controlling the morphology and facets of materials with nanometer and micrometer size has received considerable attention. For example, Fig. 9A presents various high-resolution field-emission scanning electron microscope (FE-SEM) images and the schematic drawings of goethite and hematite [39]. The morphology and

Fig. 8. Possible photo-Fenton catalytic mechanism of Ag/AgBr/ferrihydrite; the photo-generated electrons from AgBr and Ag nanoparticles can not only accelerate the redox cycle of Fe(III)/Fe(II) but also reduce the decomposition of H$_2$O$_2$ for the regeneration of Fe^{2+}/Fe(II), increasing the utilization efficiency of H$_2$O$_2$. Reproduced from Ref. [36], Copyright (2018), with permission from Elsevier.
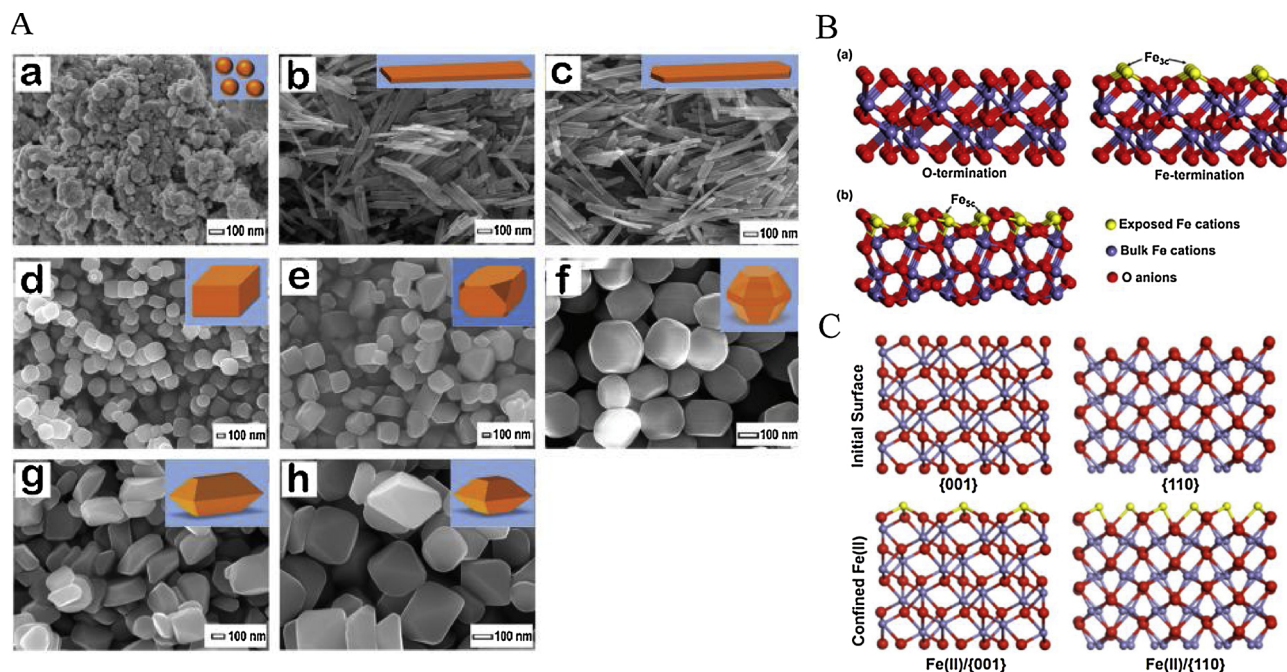
A

B

C

Fig. 9. (A). High-resolution FE-SEM images of goethite and hematite nanocrystals. (a) Goethite nanoparticles, (b) goethite nanorods, (c) hematite nanorods, (d) hematite nanocuboids, (e) hematite irregularly shaped nanocrystals, (f) hematite bitruncated dodecahedrons, (g) hematite bitruncatedelongated octahedrons, (h) hematite bitruncated octahedrons. Reproduced from Ref. [39], Copyright (2009), with permission from Royal Society of Chemistry; (B) Atomic arrangement of hematite with exposed {001} and {012} facets. (a) {001} and (b) {012} facets. Reproduced from Ref. [142], Copyright (2017), with permission from American Chemistry Society; (C) Schematic models to illustrating the confinement of Fe(II) on the {001} and {110} surfaces of hematite. Oxygen atoms are red spheres, bulk iron atoms are blue spheres, and confined ferrous iron atoms on the surfaces are yellow spheres. Reproduced from Ref. [41], Copyright (2016), with permission from Elsevier (For interpretation of the references to colour in this figure legend, the reader is referred to the web version of this article).

facets of these materials are closely related to their surface atomic configuration and coordination, which have a great influence on their physical and chemical properties. In this regard, an increasing number of studies have paid attention to controlling the specific morphologies and exposed facets of heterogeneous Fenton catalysts, which can greatly promote the activation of H_2O_2 via absorbing more Fe^{2+} and other reactive species (e.g., ascorbate) on their surfaces [39,41,92,142,157–164].

Many studies have focused on synthesizing well-defined catalysts with specific facets, especially hematite, in the field of environmental remediation in recent years [41,142,157–159]. These studies have provided the fundamental mechanisms between hematite facets and other additions (e.g., ferrous iron and ascorbate) and shed light on the design of highly efficient heterogeneous Fenton catalysts by controlling the exposed facets. For example, Huang et al. 2017 found that hematite nanoplates with {001} facets exposed exhibited better Fenton catalytic performance or a better reductive dissolution rate than hematite na-nocubes with {002} facets exposed in the presence of ascorbate [142,158]. The formation of inner-sphere iron − ascorbate complexes on the hematite facets can significantly inhibit the dissolution of sur-face-bound ferrous ions, resulting in the better stability of hematite and higher Fenton catalytic performance. In Fig. 9B [142], the Fe_{5c} sites of the {012} facets showed a worse affinity for ascorbate than the Fe_{3c} sites of the {001} facets, which is attributed to the fact that the much greater number of undercoordinated iron cations in {012} facets may present a stronger stereo-hindrance effect, hindering ascorbate complex formation. The authors also demonstrated that hematite nanorods with exposed {001} and {110} facets exhibit better confining effects with ferrous ions than nanoplates with exposed {001} facets, resulting in significant promotion of H_2O_2 decomposition and organic contaminant degradation rates [41]. The polar {110} facets can confine ferrous ions of higher density with a five-coordination binding mode and thus lower the H_2O_2 decomposition energetic span more efficiently than the

nonpolar {001} facets (six-coordination binding mode), as shown in Fig. 9C.

In addition, Dai et al. [92] noted that the ofloxacin degradation rate of $CuFeO_2$ {012} is four times higher than that of $CuFeO_2$ {110} (0.0408 vs 0.0101 min^{-1}). The results showed that the electrons from $CuFeO_2$ {012} favor the reduction of adsorbed H_2O_2 to generate $HO^{\cdot}$ due to the suitable elongation of the O—O (1.472 Å) bond length of $CuFeO_2$ compared with that of free H_2O_2 (1.468 Å). Ji et al. [85] revealed that $Bi_{25}FeO_{40}$ microcubes with {001} facet showed enhanced photo-Fenton catalytic activity due to the existence of active O atoms.

Zhong et al. [164] found that, under UVA irradiation, the catalytic activity of Fe_3O_4 in different morphologies was in the order of nano-spheres > nanoplates > nano-octahedrons ≈ nanocubes > nanorods > nano-octahedrons (by coprecipitation). The highest cata-lytic performance of Fe_3O_4 nanospheres was attributed to their smaller particle size, larger specific surface area, and greater exposure of re-active facets {111} (i.e., more Fe^{2+} species). Very recently, Xiao et al. [218] synthesized burger-like α-Fe_2O_3 catalysts via a process including oriented aggregation and Ostwald ripening, which exhibited higher photo-Fenton catalytic activity than α-Fe_2O_3 with other morphologies for the degradation of acid red G in aqueous solution. In addition, the burger-like α-Fe_2O_3 catalyst retained high catalytic activity after six experimental cycles with negligible iron leaching.

8. In situ generation of H_2O_2 in heterogeneous Fenton reaction systems

As mentioned above, in practical industrial applications, a large amount of Fe^{2+} (18–410 mmol/L) and H_2O_2 (30–6000 mmol/L) is generally required to produce sufficient $HO^{\cdot}$ for wastewater treatment, which is a major barrier to the application of this treatment [28]. In addition, the above studies demonstrated that the decomposition of H_2O_2 significantly affected the heterogeneous Fenton reactivity. Thus,
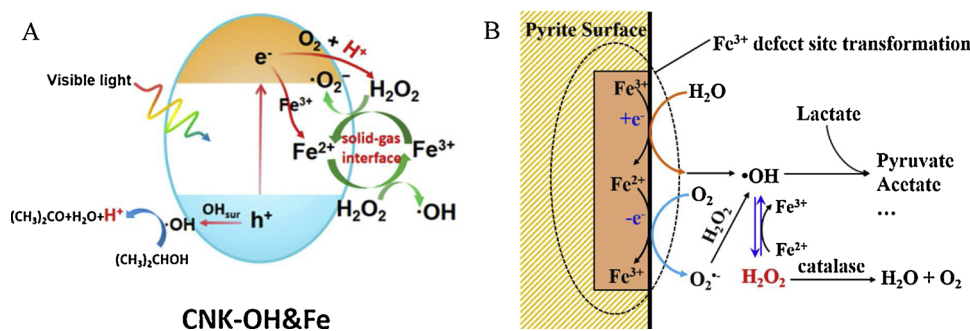
some researchers have introduced semiconductors, such as TiO_2, C_3N_4, CdS, and BiOX (X = Cl, Br, and I) to the heterogeneous Fenton system to *in situ* generate H_2O_2, which can promote the efficiency of the subsequent oxidation reaction and lower the relevant costs of H_2O_2 consumption as well [99,153–156]. Under light irradiation, the photogenerated electrons from these semiconductors can react with O_2 to generate H_2O_2 (Eq. 51), promoting the reaction with the Fe(III)/Fe(II) pair to produce $HO^·$ and $O_2^{·−}$.

$$O_2 + 2H^+ + 2e^- \rightarrow H_2O_2 \tag{51}$$

Li et al. 2016 [155] constructed an alkalinized g-C_3N_4-Fe^{3+} system (CNK−OH&Fe) to effectively convert the photocatalytic generation of H_2O_2 into $HO^·$ and $O_2^{·−}$; the system showed approximately 270 times higher reactivity than pristine C_3N_4 for the photooxidation of isopropanol. As shown in Fig. 10A, under visible light irradiation, the photo-generated electrons from g-C_3N_4 can react with O_2 to generate H_2O_2, supplying the prerequisite to initiating the Fenton process. Zhou et al. 2018 [99] constructed an in situ Fenton-like photocatalytic system driven by combining BiOBr, a benign in situ H_2O_2 producer, with $Co_xFe_yO_4$, and the reaction rate constant of this composite was 3.4 times as high as that of BiOBr under visible light irradiation.

In addition, a number of studies showed that some iron-based catalysts, such as pyrite, magnetite, and nZVI, can spontaneously in situ generate H_2O_2 [56,153,173–175]. Borda et al. 2003 [173] reported that $HO^·$ and H_2O_2 could be generated at sulfur-deficient defect sites on the pyrite surface via the reaction between adsorbed Fe^{3+} and H_2O in O_2-free water, as shown in Eqs. (52–53). According to this theory, Wang et al. 2012 [56] pointed out that pyrite can serve as a Fenton-like reagent to oxidize lactate without the addition of H_2O_2 (Fig. 10B).

$$Fe_{(pyrite)}^{3+} + H_2O_{(ads)} \rightarrow Fe_{(pyrite)}^{2+} + HO^· + H^+ \tag{52}$$

$$HO^· + HO^· \rightarrow H_2O_2 \tag{53}$$
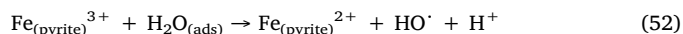
9. Recent novel advances in heterogeneous Fenton-like reactions

As mentioned above, in addition to Fe, other metals (e.g., Cu, Co, Mn, Ce, Al, Cr, and Ru) can activate H_2O_2, persulfate, or peroxymonosulfate to generate $HO^·$; these processes are known as Fenton-like reactions [219]. Fig. 11 summarized the related reactions between H_2O_2 and these metal ions. In this review, we briefly introduced some recent heterogeneous Fenton-like reactions that are of particular interest, including constructing dual reaction centers (i.e., the electron-poor center and the electron-rich center) [165–168] and synthesizing single-atom catalysts [169,170] to enhance the heterogeneous Fenton-like reactivity.

9.1. Constructing dual reaction centers on heterogeneous Fenton-like catalysts

Cu-based catalysts have received increased attention in the heterogeneous Fenton-like reactions due to the high efficiency of H_2O_2
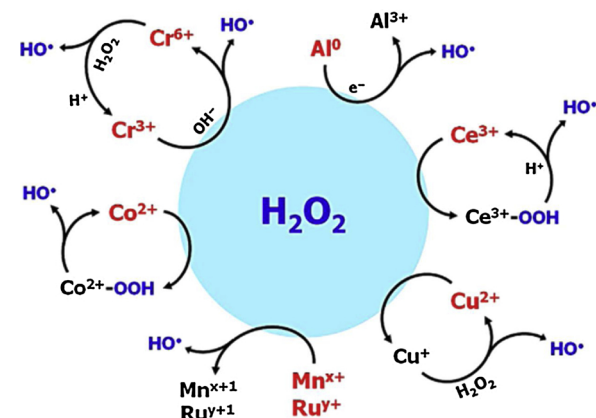

Fig. 11. Schematic illustration of H_2O_2 activation mechanisms using different nonferrous Fenton-type catalysts; the species highlighted in red indicate active Fenton catalysts. Reproduced from Ref. [219], Copyright (2014), with permission from Elsevier (For interpretation of the references to colour in this figure legend, the reader is referred to the web version of this article).

activation. For the past few years, Hu and her group have studied different single reaction center and dual reaction centers in Fenton-like systems based on Cu-containing catalysts, such as Cu-doped γ-Al_2O_3 (γ-Cu−Al_2O_3) [165], d-TiCuAl−SiO_2 [166], and C-g-C_3N_4/CuCo−Al_2O_3 (CCN/CuCo−Al_2O_3) [167], to solve one of the core issues of Fenton reactions, i.e., the low utilization efficiency of H_2O_2. In addition, the authors extended the study of dual reaction centers to metal-free Fenton-like catalysts, e.g., 4-phenoxyphenol-functionalized reduced graphene oxide nanosheets (POP-rGO NSs) [168]. These strategies can raise the utilization efficiency of H_2O_2 to approximately 90% by generating effective $HO^·$ and can achieve highly effective and stable persistent contaminant degradation at neutral pH values. For example, in mesoporous Cu-doped γ-Al_2O_3 (γ-Cu−Al_2O_3) [165], some $HO^·$ radicals are generated by the reaction of H_2O_2 with Cu^+ (Eq. 54). Meanwhile, the generated Cu^{2+} on γ-Cu−Al_2O_3 can complex with the phenolic OH group of BPA via σ bonding to form σ-Cu^{2+}−ligand complexes. H_2O_2 can react with the σ-Cu^{2+}−ligand complexes to produce one HO-adduct radical and one $HO^·$ radical and achieve the reduction of Cu^{2+} to Cu^+ at the same time, which prevents the reaction between Cu^{2+} and H_2O_2 to form less reactive $HO_2^·/O_2^{·−}$ or O_2. This study provided new insight into the design of a new type of heterogeneous Fenton-like catalyst for the degradation of some aromatic contaminants at neutral pH. However, the formation of σ-Cu^{2+}−ligand complexes strongly depends on the phenolic hydroxyl groups of aromatic contaminants. Therefore, the degradation of other contaminants will be hampered by this limitation.

In heterogeneous Fenton-like catalyst, all of the active atoms are not free metal ions, which are bound in the structure by connections with other atoms. Therefore, the outer sphere electrons no longer belong to the metal atoms only. The redistribution of these electrons might be an effective strategy to promote the reactivity of these heterogeneous
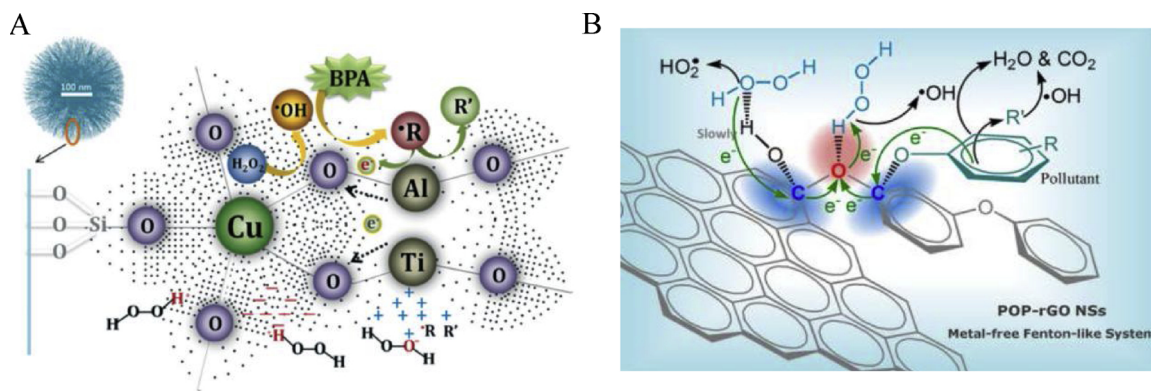
Fig. 12. (A) Fenton-like reaction mechanism on the surface of galvanic-like cells of d-TiCuAl–SiO$_2$ NNs; electron-rich center (Cu center; reduces H$_2$O$_2$ to HO˙) and electron-poor center (in the region near Ti and Al; transfers the electrons from R˙ to the Cu center). Reproduced from Ref. [166], Copyright (2016), with permission from The Royal Society of Chemistry; (B) Fenton-like reaction mechanism of POP-rGO NSs; the electron-poor center around C captures electrons from the adsorbed contaminants and transfers them to the electron-rich area via the C − O–C bridge. Reproduced from Ref. [168], Copyright (2018), with permission from American Chemistry Society.

Fenton-like catalysts. Recently, Lyu et al. [166] synthesized a novel d-TiCuAl–SiO$_2$ nanocatalysts consisting of Cu-, Ti-, and Al-doped dandelion-like silica nanospheres. Cu, Ti, and Al were incorporated in the lattice of silica nanospheres to substitute Si, resulting in a nonuniform distribution of electrons due to the different electronegativities of the metals. In this Fenton-like reaction process (Fig. 12A), H$_2$O$_2$ was reduced to HO˙ by the electrons around electron-rich Cu centers, while R˙ from the degradation of organic contaminants, rather than H$_2$O$_2$, donated electrons to the electron-poor centers (i.e., in the region near Ti and Al); these electrons were rapidly delivered to the Cu centers due to the higher electronegativity of Cu, avoiding the oxidation of H$_2$O$_2$. Because of the special Fenton-like reaction process, almost all of the H$_2$O$_2$ was used to generate HO˙ for the degradation of contaminants, resulting in extremely high utilization efficiency of H$_2$O$_2$.

However, whether a homogeneous or heterogeneous Fenton-like process is used, the reaction is always restricted by the rate-limiting step due to the low reaction rate constant for the reduction of M$^{(n+m)+}$ to M^{n+}. Therefore, Lyu et al. 2018 synthesized 4-phenoxyphenol-functionalized reduced graphene oxide nanosheets (POP-rGO NSs) through surface complexation and copolymerization and constructed a highly effective and stable metal-free Fenton-like reaction center [168]. As shown in Fig. 12B, around the electron-rich O center, H$_2$O$_2$ can be effectively decomposed to HO˙, while the electron-poor center around C captures electrons from the adsorbed contaminants and transfers them to the electron-rich area via the C−O−C bridge. In addition, DFT analysis revealed that surface complexation of POP with rGO via C−O−C bridges enables the nonuniform distribution of electrons on the surface of the catalyst, producing dual reaction centers around the C−O−C bridges. This study sheds light on the design of effective and economic Fenton-like catalysts for environmental remediation. In addition, they found that the dual reaction centers in these reaction systems can extend the suitable pH to near-neutral condition.

9.2. Synthesizing novel single-atom catalysis-based heterogeneous Fenton-like catalysts

The application of catalysts with ultra-small clusters and single-atom sites has attracted great interest in different areas, such as the oxygen reduction reaction, volatile organic compound removal, and electrocatalysis, because of their high atom-utilization efficiency [220–223]. For example, single-atom Cu−N@graphene catalyst with a high density of active sites was achieved with a metal loading up to 8.5 wt %, suggesting the promising potential for practical applications

[222]. Very recently, some researchers found that single-atom catalysts with atomically distributed active metal centers (e.g., Fe and Co) presented high Fenton/Fenton-like reactivity by achieving maximum atom efficiency [169,170].

An et al. [169] synthesized a catalyst with ultra-small clusters and single-atom Fe sites embedded in graphitic carbon nitride (FeN$_x$/g-C$_3$N$_4$) via one-step pyrolysis for advanced oxidation processes. In this catalyst, g-C$_3$N$_4$, with high-density homogeneous N atoms and "six-fold cavities" for firmly trapping transition metals, is promising support to stabilize high-density ultra-small metal clusters and single-atom Fe sites. The majority of Fe atoms are in the Fe(II) state for all composites, which can promote the activation of H$_2$O$_2$ to generate HO˙, resulting in excellent removal efficiency for various typical organics.

Li et al. [170] synthesized highly reactive and stable Fenton-like catalysts with dual reaction sites by anchoring single cobalt atoms on porous N-doped graphene for the catalytic oxidation of BPA via the activation of peroxymonosulfate. In this single-Co-atom catalyst, the CoN$_4$ site with a single Co atom serves as the active site with optimal binding energy for PMS activation, while the adjacent pyrrolic N site adsorbs BPA (Fig. 13), which greatly reduces the migration distance for singlet oxygen produced from PMS activation, improving the Fenton-like catalytic performance.

10. Conclusion and prospects

Heterogeneous Fenton reactions have been rapidly developed due to the excellent stability and reusability of the catalysts, wide application pH range, high oxidation efficiency and low operating costs, which make these reactions stand out among various AOPs. In terms of the drawbacks of heterogeneous Fenton reactions, i.e., low generation of Fe(II) and high consumption of H$_2$O$_2$, a number of studies have proposed various strategies and their underlying mechanisms for enhancing heterogeneous Fenton reactivity through the following means: injecting additional electrons from external electric fields, electron-rich materials, semiconductors, or plasmonic materials, or doping metals in heterogeneous Fenton catalysts to accelerate the generation of Fe(II) and promote the decomposition of H$_2$O$_2$; combining ultrasound, electricity, semiconductors, and iron-based catalysts in the system to in situ generate H$_2$O$_2$; controlling the morphologies and exposed facets of catalysts to promote the decomposition of H$_2$O$_2$. In addition, some recent novel advances in heterogeneous Fenton-like reactions that are of particular interest, including constructing dual reaction centers and synthesizing single-atom catalysis, can significantly enhance
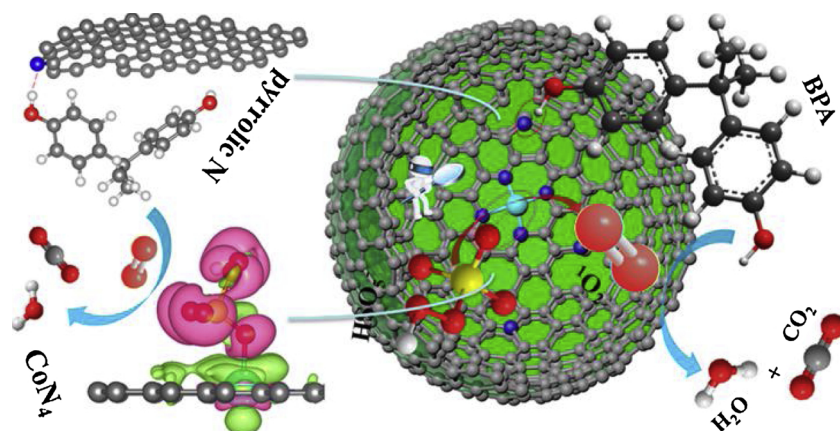
Fig. 13. Fenton-like reaction mechanism of the as-prepared catalyst; CoN$_4$ site with a single Co atom serves as the active site for PMS activation, while the adjacent pyrrolic N site adsorbs BPA. Reproduced from Ref. [170], Copyright (2018), with permission from American Chemistry Society.

heterogeneous Fenton-like reactivity. Based on the current studies, the following suggestions are proposed for future work.

1 Single-atom catalysts, with atomically distributed active metal centers, have recently emerged as a new research frontier in various catalytic reactions for maximum atom efficiency; however, few developments have involved Fenton/Fenton-like reactions. Some transition metals, such as Fe, Co, Cu, and Mn, can behave as heterogeneous Fenton/Fenton-like catalysts since they can motivate H_2O_2 to generate HO$^{\cdot}$. Therefore, single-atom catalysts containing these transition metals with homogeneous active metal sites may be novel and effective heterogeneous Fenton/Fenton-like catalysts for wastewater treatment.

2 As mentioned above, combining carbon materials with iron catalysts can significantly enhance the heterogeneous Fenton reactivity for the degradation of organic contaminants in wastewater because carbon materials can act as excellent "electron shuttles" to mediate electron-transfer reactions. In the soil environment, natural iron minerals (e.g., ferrihydrite, pyrite, and magnetite) and natural carbon particles (e.g., biochar) are ubiquitous. In addition, natural pyrite and magnetite can spontaneously generate H_2O_2 in situ. Therefore, it is worth studying the possible reaction process in the presence of coexisting natural iron minerals and carbon materials for the self- remediation of soil pollution.

3 In both conventional homogeneous Fenton reactions and heterogeneous Fenton-like reactions, the redox reaction of the metal ions by H_2O_2 is always the rate-limiting step. In addition, the metal-containing Fenton reaction can inevitably cause secondary pollution owing to the production of metal-containing sludge or metal leaching, which narrow the application of Fenton reactions for environmental remediation. Therefore, the development of metal-free Fenton-like catalysts may be a new trend for environmental remediation.

4 The heterogeneous Fenton/Fenton-like reaction process has been systematically studied at the laboratory level by a large number of researchers; however, the application of such processes to practical industrial wastewater is still a challenge. Therefore, combining heterogeneous Fenton/Fenton-like reaction processes with other mature wastewater treatment techniques must be further studied.

References

[1] L. Ye, J. Liu, C. Gong, L. Tian, T. Peng, L. Zan, ACS Catal. 2 (2012) 1677–1683.
[2] M. Cheng, C. Lai, Y. Liu, G. Zeng, D. Huang, C. Zhang, L. Qin, L. Hu, C. Zhou, W. Xiong, Coord. Chem. Rev. 368 (2018) 80–92.
[3] S. Rahim Pouran, A.A. Abdul Raman, W.M.A. Wan Daud, J. Cleaner Prod. 64 (2014) 24–35.
[4] N. Mishra, R. Reddy, A. Kuila, A. Rani, A. Nawaz, S. Pichiah, Curr. World Environ. 12 (2017) 469–489.
[5] M.V. Bagal, P.R. Gogate, Ultrason. Sonochem. 21 (2014) 1–14.
[6] A. Dhakshinamoorthy, S. Navalon, M. Alvaro, H. Garcia, ChemSusChem 5 (2012) 46–64.
[7] N. Wang, T. Zheng, G. Zhang, P. Wang, J. Environ. Chem. Eng. 4 (2016) 762–787.
[8] S. Garcia-Segura, L.M. Bellotindos, Y.-H. Huang, E. Brillas, M.-C. Lu, J. Taiwan Inst. Chem. Eng. 67 (2016) 211–225.
[9] M. Munoz, Z.M. de Pedro, J.A. Casas, J.J. Rodriguez, Appl. Catal. B: Environ. 176-177 (2015) 249–265.
[10] J.J. Pignatello, E. Oliveros, A. MacKay, Crit. Rev. Env. Sci. Tec. 36 (2006) 1–84.
[11] Y. Zhu, R. Zhu, Y. Xi, T. Xu, L. Yan, J. Zhu, G. Zhu, H. He, Chem. Eng. J. 346 (2018) 567–577.
[12] A.N. Soon, B.H. Hameed, Desalination 269 (2011) 1–16.
[13] P.V. Nidheesh, RSC Adv. 5 (2015) 40552–40577.
[14] E.G. Garrido-Ramírez, B.K.G. Theng, M.L. Mora, Appl. Clay Sci. 47 (2010) 182–192.
[15] J. He, X. Yang, B. Men, D. Wang, J. Environ. Sci. China (China) 39 (2016) 97–109.
[16] T. Xu, R. Zhu, G. Zhu, J. Zhu, X. Liang, Y. Zhu, H. He, Appl. Catal. B: Environ. 212 (2017) 50–58.
[17] R. Cervellati, K. Höner, C. Neddens, S. Costa, Helvetica Chim. Acta 84 (2001) 3533–3547.
[18] S. Rahim Pouran, A.R. Abdul Aziz, W.M.A. Wan Daud, J. Ind. Eng. Chem. 21 (2015) 53–69.
[19] A. Babuponnusami, K. Muthukumar, J. Environ. Chem. Eng. 2 (2014) 557–572.
[20] S. Giannakis, M.I. Polo López, D. Spuhler, J.A. Sánchez Pérez, P. Fernández Ibáñez, C. Pulgarin, Appl. Catal. B: Environ. 199 (2016) 199–223.
[21] M. Hartmann, S. Kullmann, H. Keller, J. Mater. Chem. 20 (2010) 9002–9017.
[22] S. Navalon, A. Dhakshinamoorthy, M. Alvaro, H. Garcia, ChemSusChem 4 (2011) 1712–1730.
[23] S. Navalon, M. Alvaro, H. Garcia, Appl. Catal. B: Environ. 99 (2010) 1–26.
[24] J. Herney-Ramirez, M.A. Vicente, L.M. Madeira, Appl. Catal. B: Environ. 98 (2010) 10–26.
[25] P.V. Nidheesh, R. Gandhimathi, S.T. Ramesh, Environ. Sci. Pollut. Res. Int. 20 (2013) 2099–2132.
[26] M. Usman, K. Hanna, S. Haderlein, Sci. Total Environ. 569-570 (2016) 179–190.
[27] A.V. Vorontsov, J. Hazard. Mater. (2018).
[28] M. Xing, W. Xu, C. Dong, Y. Bai, J. Zeng, Y. Zhou, J. Zhang, Y. Yin, Chem. 4 (2018) 1359–1372.
[29] T. Valdés-Solís, P. Valle-Vigón, S. Álvarez, G. Marbán, A.B. Fuertes, Catal. Commun. 8 (2007) 2037–2042.
[30] N.A. Zubir, C. Yacou, J. Motuzas, X. Zhang, X.S. Zhao, J.C. Diniz da Costa, Chem.

Commun. (Camb.) 51 (2015) 9291–9293.

[31] D. Du, W. Shi, L. Wang, J. Zhang, Appl. Catal. B: Environ. 200 (2017) 484–492.

[32] R.C. Costa, M.F. Lelis, L.C. Oliveira, J.D. Fabris, J.D. Ardisson, R.R. Rios, C.N. Silva, R.M. Lago, J. Hazard. Mater. 129 (2006) 171–178.

[33] X.S. Nguyen, G. Zhang, X. Yang, ACS Appl. Mater. Inter. 9 (2017) 8900–8909.

[34] P.V. Nidheesh, R. Gandhimathi, S. Velmathi, N.S. Sanjini, RSC Adv. 4 (2014) 5698–5708.

[35] T. Xu, R. Zhu, J. Liu, Q. Zhou, J. Zhu, X. Liang, Y. Xi, H. He, J. Mol. Catal. A Chem. 424 (2016) 393–401.

[36] Y. Zhu, R. Zhu, L. Yan, H. Fu, Y. Xi, H. Zhou, G. Zhu, J. Zhu, H. He, Appl. Catal. B: Environ. 239 (2018) 280–289.

[37] X. Zhang, Y. Chen, N. Zhao, H. Liu, Y. Wei, RSC Adv. 4 (2014) 21575–21583.

[38] G.K. Pradhan, N. Sahu, K.M. Parida, RSC Adv. 3 (2013) 7912–7920.

[39] A.K. Patra, S.K. Kundu, A. Bhaumik, D. Kim, Nanoscale 8 (2016) 365–377.

[40] C. Jaramillo-Páez, J.A. Navío, M.C. Hidalgo, A. Bouziani, M.E. Azzouzi, J. Photochem. Photobiol. A: Chem. 332 (2017) 521–533.

[41] X. Huang, X. Hou, J. Zhao, L. Zhang, Appl. Catal. B: Environ. 181 (2016) 127–137.

[42] X. Chen, F. Chen, F. Liu, X. Yan, W. Hu, G. Zhang, L. Tian, Q. Xia, X. Chen, Catal. Sci. Technol. 6 (2016) 4184–4191.

[43] J. Xu, Y. Li, B. Yuan, C. Shen, M. Fu, H. Cui, W. Sun, Chem. Eng. J. 291 (2016) 174–183.

[44] Y. Wang, M. Liang, J. Fang, J. Fu, X. Chen, Chemosphere 182 (2017) 468–476.

[45] X. Hou, X. Huang, F. Jia, Z. Ai, J. Zhao, L. Zhang, Environ. Sci. Technol. 51 (2017) 5118–5126.

[46] L. Krumina, G. Lyngsie, A. Tunlid, P. Persson, Environ. Sci. Technol. 51 (2017) 9053–9061.

[47] H. Jin, X. Tian, Y. Nie, Z. Zhou, C. Yang, Y. Li, L. Lu, Environ. Sci. Technol. 51 (2017) 12699–12706.

[48] D. Fang, Y. Yu, Z. Xu, J. Liang, L. Zhou, Sci. Eng. Comp. Mater. 25 (2018) 9–15.

[49] S. Su, Y. Liu, X. Liu, W. Jin, Y. Zhao, Chemosphere 218 (2019) 83–92.

[50] Z. Xu, M. Zhang, J. Wu, J. Liang, L. Zhou, B. L, Water Sci. Technol. 68 (2013) 2178–2185.

[51] D. He, Y. Chen, Y. Situ, L. Zhong, H. Huang, Appl. Surf. Sci. 425 (2017) 862–872.

[52] M. Sheydaei, S. Aber, A. Khataee, J. Mol. Catal. A Chem. 392 (2014) 229–234.

[53] X. Wang, C. Liu, X. Li, F. Li, S. Zhou, J. Hazard. Mater. 153 (2008) 426–433.

[54] Y. Ma, B. Wang, Q. Wang, S. Xing, Chem. Eng. J. 354 (2018) 75–84.

[55] W. Liu, Y. Wang, Z. Ai, L. Zhang, ACS Appl. Mater. Inter. 7 (2015) 28534–28544.

[56] W. Wang, Y. Qu, B. Yang, X. Liu, W. Su, Chemosphere 86 (2012) 376–382.

[57] Y. Zhang, K. Zhang, C. Dai, X. Zhou, H. Si, Chem. Eng. J. 244 (2014) 438–445.

[58] Z.-H. Diao, X.-R. Xu, D. Jiang, G. Li, J.-J. Liu, L.-J. Kong, L.-Z. Zuo, J. Hazard. Mater. 327 (2017) 108–115.

[59] W.M. Wang, J. Song, X. Han, J. Hazard. Mater. 262 (2013) 412–419.

[60] X. Li, Y. Zhang, Y. Xie, Y. Zeng, P. Li, T. Xie, Y. Wang, J. Hazard. Mater. 344 (2018) 689–697.

[61] G.C. Yang, S.-C. Huang, C.-L. Wang, Y.-S. Jen, Chemosphere 159 (2016) 282–292.

[62] Y. Zhu, C. Zeng, R. Zhu, Y. Xu, X. Wang, H. Zhou, J. Zhu, H. He, J. Environ. Sci. China (China) 80 (2019) 208–217.

[63] Y. Deng, M. Xing, J. Zhang, Appl. Catal. B: Environ. 211 (2017) 157–166.

[64] J. Bai, Y. Liu, X. Yin, H. Duan, J. Ma, Appl. Surf. Sci. 416 (2017) 45–50.

[65] M. Laipan, H. Fu, R. Zhu, L. Sun, J. Zhu, H. He, Sci. Rep. 7 (2017) 7277.

[66] M. Laipan, R. Zhu, J. Zhu, H. He, J. Mol. Catal. A Chem. 415 (2016) 9–16.

[67] T. Xu, R. Zhu, J. Zhu, X. Liang, Y. Liu, Y. Xu, H. He, Appl. Clay Sci. 129 (2016) 27–34.

[68] T. Xu, R. Zhu, J. Zhu, X. Liang, Y. Liu, Y. Xu, H. He, Catal. Sci. Technol. 6 (2016) 4116–4123.

[69] H. Fida, G. Zhang, S. Guo, A. Naeem, J. Colloid Interface Sci. 490 (2017) 859–868.

[70] G.-T. Wei, C.-Y. Fan, L.-Y. Zhang, R.-C. Ye, T.-Y. Wei, Z.-F. Tong, Catal. Commun. 17 (2012) 184–188.

[71] B. Iurascu, I. Siminiceanu, D. Vione, M. Vicente, A. Gil, Water Res. 43 (2009) 1313–1322.

[72] Y. Liu, Y. Mao, X. Tang, Y. Xu, C. Li, F. Li, Chinese J. Catal. 38 (2017) 1726–1735.

[73] J. Deng, H. Dong, C. Zhang, Z. Jiang, Y. Cheng, K. Hou, L. Zhang, C. Fan, Sep. Purif. Technol. 202 (2018) 130–137.

[74] Y. Mu, F. Jia, Z. Ai, L. Zhang, Environ. Sci-Nano 4 (2017) 27–45.

[75] S. Zhang, D. Wang, X. Zhang, P. Fan, C.L.E.A.N.- Soil, Air, Water 42 (2014) 609–616.

[76] Y. Xi, Z. Sun, T. Hreid, G.A. Ayoko, R.L. Frost, Chem. Eng. J. 247 (2014) 66–74.

[77] H. Wu, Z. Ai, L. Zhang, Water Res. 52 (2014) 92–100.

[78] L. Ma, H. He, R. Zhu, J. Zhu, I.D.R. Mackinnon, Y. Xi, Catal. Sci. Technol. 6 (2016) 6066–6075.

[79] M.B. Kasiri, H. Aleboyeh, A. Aleboyeh, Appl. Catal. B: Environ. 84 (2008) 9–15.

[80] M. Dükkancı, G. Gündüz, S. Yılmaz, R. Prihod'ko, J. Hazard. Mater. 181 (2010) 343–350.

[81] X. Qian, Y. Wu, M. Kan, M. Fang, D. Yue, J. Zeng, Y. Zhao, Appl. Catal. B: Environ. 237 (2018) 513–520.

[82] J. An, G. Zhang, R. Zheng, P. Wang, J. Environ. Sci. China (China) 48 (2016) 218–229.

[83] K. Rusevova, R. Köferstein, M. Rosell, H.H. Richnow, F.-D. Kopinke, A. Georgi, Chem. Eng. J. 239 (2014) 322–331.

[84] L. Ren, S.Y. Lu, J.Z. Fang, Y. Wu, D.Z. Chen, L.Y. Huang, Y.F. Chen, C. Cheng, Y. Liang, Z.Q. Fang, Catal. Today 281 (2017) 656–661.

[85] W. Ji, M. Li, G. Zhang, P. Wang, Dalton Trans. 46 (2017) 10586–10593.

[86] N. Wang, L. Zhu, M. Lei, Y. She, M. Cao, H. Tang, ACS Catal. 1 (2011) 1193–1202.

[87] C. Cai, Z. Zhang, J. Liu, N. Shan, H. Zhang, D.D. Dionysiou, Appl. Catal. B: Environ. 182 (2016) 456–468.

[88] S. Wu, X. Shen, G. Zhu, H. Zhou, Z. Ji, K. Chen, A. Yuan, Appl. Catal. B: Environ.

184 (2016) 328–336.

[89] F. He, Y. Ji, Y. Wang, Y. Zhang, J. Taiwan Inst. Chem. Eng. 80 (2017) 553–562.

[90] Y. Nie, L. Zhang, Y.Y. Li, C. Hu, J. Hazard. Mater. 294 (2015) 195–200.

[91] D. Sannino, V. Vaiano, L.A. Isupova, P. Ciambelli, Chem. Eng. Trans. 25 (2011) 1013–1018.

[92] C. Dai, X. Tian, Y. Nie, H.M. Lin, C. Yang, B. Han, Y. Wang, Environ. Sci. Technol. 52 (2018) 6518–6525.

[93] Y. Ding, W. Huang, Z. Ding, G. Nie, H. Tang, Sep. Purif. Technol. 168 (2016) 223–231.

[94] X. Guo, K. Wang, D. Li, J. Qin, Appl. Surf. Sci. 420 (2017) 792–801.

[95] S. Guo, G. Zhang, J.C. Yu, J. Colloid Interface Sci. 448 (2015) 460–466.

[96] H. Zhou, X. Yue, H. Lv, L. Kong, Z. Ji, X. Shen, Ceram. Int. 44 (2018) 7240–7244.

[97] L. Wei, Y. Zhang, S. Chen, L. Zhu, X. Liu, L. Kong, L. Wang, J. Environ. Sci. China (China) 76 (2019) 188–198.

[98] Y. Yao, G. Wu, F. Lu, S. Wang, Y. Hu, J. Zhang, W. Huang, F. Wei, Environ. Sci. Pollut. Res. Int. 23 (2016) 21833–21845.

[99] T. Zhou, Y. Xu, X. Wang, S. Huang, M. Xie, J. Xia, L. Huang, H. Xu, H. Li, Catal. Sci. Technol. 8 (2018) 551–561.

[100] Z. Ma, L. Ren, S. Xing, Y. Wu, Y. Gao, J. Phys. Chem. C 119 (2015) 23068–23074.

[101] X.-j. Yang, X.-m. Xu, J. Xu, Y.-f. Han, J. Am. Chem. Soc. 135 (2013) 16058–16061.

[102] X.-j. Yang, X.-m. Xu, X.-c. Xu, J. Xu, H.-l. Wang, R. Semiat, Y.-f. Han, Catal. Today 276 (2016) 85–96.

[103] J. He, X. Yang, B. Men, L. Yu, D. Wang, J. Mol. Catal. A Chem. 408 (2015) 179–188.

[104] X. Hu, B. Liu, Y. Deng, H. Chen, S. Luo, C. Sun, P. Yang, S. Yang, Appl. Catal. B: Environ. 107 (2011) 274–283.

[105] M.L. Kremer, Phys. Chem. Chem. Phys. 1 (1999) 3595–3605.

[106] S.H. Bossmann, E. Oliveros, S. Göb, S. Siegwart, E.P. Dahlen, J. Leon Payawan, M. Straub, M. Wörner, A.M. Braun, J. Phys. Chem. A 102 (1998) 5542–5550.

[107] E. Sires, M.A. Brillas, M.A. Oturan, M. Rodrigo, Panizza, Environ. Sci. Pollut. Res. Int. 21 (2014) 8336–8367.

[108] S.O. Ganiyu, M. Zhou, C.A. Martínez-Huitle, Appl. Catal. B: Environ. 235 (2018) 103–129.

[109] A. Zhang, Z. Gu, W. Chen, Q. Li, G. Jiang, Environ. Sci. Pollut. Res. Int. 25 (2018) 28907–28916.

[110] S. Li, G. Zhang, W. Zhang, H. Zheng, W. Zhu, N. Sun, Y. Zheng, P. Wang, Chem. Eng. J. 326 (2017) 756–764.

[111] C. Wang, Y. Shih, Sep. Purif. Technol. 140 (2015) 6–12.

[112] X. Zhong, L. Xiang, S. Royer, S. Valange, J. Barrault, H. Zhang, J. Chem. Technol. Biot. 86 (2011) 970–977.

[113] Q. Huang, M. Cao, Z. Ai, L. Zhang, Appl. Catal. B: Environ. 162 (2015) 319–326.

[114] W. Shen, F. Lin, X. Jiang, H. Li, Z. Ai, L. Zhang, Chem. Eng. J. 308 (2017) 880–888.

[115] L. Zhu, Z. Ai, W. Ho, L. Zhang, Sep. Purif. Technol. 108 (2013) 159–165.

[116] J. Shi, Z. Ai, L. Zhang, Water Res. 59 (2014) 145–153.

[117] T.J.S. And, A.T. Stone, Environ. Sci. Technol. 36 (2016) 5172–5183.

[118] L. Deng, Z. Shi, Z. Zou, S. Zhou, Environ. Sci. Pollut. Res. Int. 24 (2017) 11536–11548.

[119] H. Zhang, T. Tong, W.-H. Cao, J.-G. Chen, D.-R. Jin, J.-R. Cheng, J. Sol-Gel Sci. Techn. 75 (2015) 481–485.

[120] S.-P. Sun, X. Zeng, C. Li, A.T. Lemley, Chem. Eng. J. 244 (2014) 44–49.

[121] X. Xue, K. Hanna, C. Despas, F. Wu, N. Deng, J. Mol. Catal. A Chem. 311 (2009) 29–35.

[122] T.J. Strathmann, A.T. Stone, Environ. Sci. Technol. 36 (2002) 5172–5183.

[123] Y. Qin, L. Zhang, T. An, ACS Appl. Mater. Inter. 9 (2017) 17115–17124.

[124] D. Xu, Y. Zhang, F. Cheng, P. Dai, J. Taiwan Inst. Chem. Eng. 60 (2016) 376–382.

[125] Z. Yang, A. Yu, C. Shan, G. Gao, B. Pan, Water Res. 137 (2018) 37–46.

[126] J. Ma, M. Yang, F. Yu, J. Chen, J. Colloid Interface Sci. 444 (2015) 24–32.

[127] G. Fang, C. Liu, J. Gao, D.D. Dionysiou, D. Zhou, Environ. Sci. Technol. 49 (2015) 5645–5653.

[128] G. Fang, J. Gao, C. Liu, D.D. Dionysiou, Y. Wang, D. Zhou, Environ. Sci. Technol. 48 (2014) 1902–1910.

[129] J. Ma, Q. Yang, Y. Wen, W. Liu, Appl. Catal. B: Environ. 201 (2017) 232–240.

[130] S.H. Yoo, D. Jang, H.-I. Joh, S. Lee, J. Mater. Chem. A Mater. Energy Sustain. 5 (2017) 748–755.

[131] C. Dong, J. Ji, B. Shen, M. Xing, J. Zhang, Environ. Sci. Technol. 52 (2018) 11297–11308.

[132] J. Liu, C. Dong, Y. Deng, J. Ji, S. Bao, C. Chen, B. Shen, J. Zhang, M. Xing, Water Res. 145 (2018) 312–320.

[133] L. Chen, J. Ma, X. Li, J. Zhang, J. Fang, Y. Guan, P. Xie, Environ. Sci. Technol. 45 (2011) 3925–3930.

[134] X. Wu, X. Gu, S. Lu, Z. Qiu, Q. Sui, X. Zang, Z. Miao, M. Xu, Sep. Purif. Technol. 147 (2015) 186–193.

[135] J. Zou, J. Ma, L. Chen, X. Li, Y. Guan, P. Xie, C. Pan, Environ. Sci. Technol. 47 (2013) 11685–11691.

[136] L. Chen, X. Li, J. Zhang, J. Fang, Y. Huang, P. Wang, J. Ma, Environ. Sci. Technol. 49 (2015) 10373–10379.

[137] J. Bolobajev, M. Trapido, A. Goi, Chem. Eng. J. 281 (2015) 566–574.

[138] D. Han, J. Wan, Y. Ma, Y. Wang, M. Huang, Y. Chen, D. Li, Z. Guan, Y. Li, Chem. Eng. J. 256 (2014) 316–323.

[139] G. Liu, X. Li, B. Han, L. Chen, L. Zhu, L.C. Campos, J. Hazard. Mater. 322 (2017) 461–468.

[140] X. Hou, X. Huang, Z. Ai, J. Zhao, L. Zhang, J. Hazard. Mater. 310 (2016) 170–178.

[141] X. Hou, W. Shen, X. Huang, Z. Ai, L. Zhang, J. Hazard. Mater. 308 (2016) 67–74.

[142] X. Huang, X. Hou, F. Jia, F. Song, J. Zhao, L. Zhang, ACS Appl. Mater. Inter. 9 (2017) 8751–8758.

[143] H. Lee, H.J. Lee, J. Seo, H.E. Kim, Y.K. Shin, J.H. Kim, C. Lee, Environ. Sci.

Technol. 50 (2016) 8231–8238.

[144] X. Wu, X. Gu, S. Lu, Z. Qiu, Q. Sui, X. Zang, Z. Miao, M. Xu, M. Danish, J. Chem. Technol. Biot. 91 (2016) 1280–1289.

[145] Z. Xu, C. Huang, L. Wang, X. Pan, L. Qin, X. Guo, G. Zhang, Ind. Eng. Chem. Res. 54 (2015) 4593–4602.

[146] Y. Hou, Y. Wang, H. Yuan, H. Chen, G. Chen, J. Shen, L. Li, J. Nanopart. Res. 18 (2016) 343.

[147] W. Shi, D. Du, B. Shen, C. Cui, L. Lu, L. Wang, J. Zhang, ACS Appl. Mater. Inter. 8 (2016) 20831–20838.

[148] K. Uma, N. Arjun, G.-T. Pan, T.C.K. Yang, Appl. Surf. Sci. 425 (2017) 377–383.

[149] A.C. Silva, D.Q. Oliveira, L.C. Oliveira, A.S. Anastacio, T.C. Ramalho, J.H. Lopes, H.W. Carvalho, C.E.R. Torres, Appl. Catal. A Gen. 357 (2009) 79–84.

[150] X.S. Nguyen, K.D. Ngo, J. Surf. Eng. Mater. Adv. Technol. 8 (2017) 1.

[151] I.R. Guimaraes, A. Giroto, L.C. Oliveira, M.C. Guerreiro, D.Q. Lima, J.D. Fabris, Appl. Catal. B: Environ. 91 (2009) 581–586.

[152] Y. Diao, Z. Yan, M. Guo, X. Wang, J. Hazard. Mater. 344 (2018) 829–838.

[153] A. Asghar, A.A. Abdul Raman, W.M.A. Wan Daud, J. Cleaner Prod. 87 (2015) 826–838.

[154] Z. Jiang, L. Wang, J. Lei, Y. Liu, J. Zhang, Appl. Catal. B: Environ. 241 (2019) 367–374.

[155] Y. Li, S. Ouyang, H. Xu, X. Wang, Y. Bi, Y. Zhang, J. Ye, J. Am. Chem. Soc. 138 (2016) 13289–13297.

[156] G.-h. Moon, S. Kim, Y.-J. Cho, J. Lim, D.-h. Kim, W. Choi, Appl. Catal. B: Environ. 218 (2017) 819–824.

[157] X. Huang, X. Hou, X. Zhang, K.M. Rosso, L. Zhang, Environ. Sci-Nano 5 (2018) 1790-18-6.

[158] X. Huang, X. Hou, F. Song, J. Zhao, L. Zhang, J. Phys. Chem. C 121 (2017) 1113–1121.

[159] H. Li, J. Shang, Z. Yang, W. Shen, Z. Ai, L. Zhang, Environ. Sci. Technol. 51 (2017) 5685–5694.

[160] J.Y. Chan, S.Y. Ang, E.Y. Ye, M. Sullivan, J. Zhang, M. Lin, Phys. Chem. Chem. Phys. Pccp 17 (2015) 25333.

[161] X. Wang, J. Wang, Z. Cui, S. Wang, M. Cao, RSC Adv. 4 (2014) 34387.

[162] C. Zang, X. Zhang, S. Hu, F. Chen, Appl. Catal. B: Environ. 216 (2017) 106–113.

[163] Y. Zhao, F. Pan, H. Li, T. Niu, G. Xu, W. Chen, J. Mater. Chem. A Mater. Energy Sustain. 1 (2013) 7242.

[164] Y. Zhong, L. Yu, Z.F. Chen, H. He, F. Ye, G. Cheng, Q. Zhang, ACS Appl. Mater. Inter. 9 (2017) 29203–29212.

[165] L. Lyu, L. Zhang, Q. Wang, Y. Nie, C. Hu, Environ. Sci. Technol. 49 (2015) 8639–8647.

[166] L. Lyu, L. Zhang, C. Hu, Environ. Sci-Nano 3 (2016) 1483–1492.

[167] L. Lyu, L. Zhang, G. He, H. He, C. Hu, J. Mater. Chem. A Mater. Energy Sustain. 5 (2017) 7153–7164.

[168] L. Lyu, G. Yu, L. Zhang, C. Hu, Y. Sun, Environ. Sci. Technol. 52 (2018) 747–756.

[169] S. An, G. Zhang, T. Wang, W. Zhang, K. Li, C. Song, J.T. Miller, S. Miao, J. Wang, X. Guo, ACS Nano 12 (2018) 9441–9450.

[170] X. Li, X. Huang, S. Xi, S. Miao, J. Ding, W. Cai, S. Liu, X. Yang, H. Yang, J. Gao, J. Wang, Y. Huang, T. Zhang, B. Liu, J. Am. Chem. Soc. 140 (2018) 12469–12475.

[171] Y. Qin, G. Li, Y. Gao, L. Zhang, Y.S. Ok, T. An, Water Res. 137 (2018) 130–143.

[172] R. Huang, Z. Fang, X. Yan, W. Cheng, Chem. Eng. J. 197 (2012) 242–249.

[173] M.J. Borda, A.R. Elsetinow, D.R. Strongin, M.A. Schoonen, Geochim. Cosmochim. Acta 67 (2003) 935–939.

[174] G.D. Fang, D.M. Zhou, D.D. Dionysiou, J. Hazard. Mater. 250-251 (2013) 68–75.

[175] P. Zhang, S. Yuan, Geochim. Cosmochim. Acta 218 (2017) 153–166.

[176] H. Zeng, X. Liu, T. Wei, X. Li, T. Liu, X. Min, Q. Zhu, X. Zhao, J. Li, RSC Adv. 7 (2017) 23787–23792.

[177] C. Ruales-Lonfat, J.F. Barona, A. Sienkiewicz, M. Bensimon, J. Vélez-Colmenares, N. Benítez, C. Pulgarín, Appl. Catal. B: Environ. 166-167 (2015) 497–508.

[178] Y. Xu, M.A.A. Schoonen, Am. Miner. 85 (2000) 543–556.

[179] D. Beydoun, R. Amal, G. Low, S. McEvoy, J. Mol. Catal. A Chem. 180 (2002) 193–200.

[180] S. Ren, C. Chen, Y. Zhou, Q. Dong, H. Ding, Res. Chem. Intermed. 43 (2016) 3307–3323.

[181] Y.H. Chen, F.A. Li, J. Colloid Interface Sci. 347 (2010) 277–281.

[182] D.M. Sherman, Geochim. Cosmochim. Acta 69 (2005) 3249–3255.

[183] M. Bronold, Y. Tomm, W. Jaegermann, Surf. Sci. 314 (1994) L931–L936.

[184] M. Enhessari, M.K. Razi, L. Etemad, A. Parviz, M. Sakhaei, J. Exp. Nanosci. 9 (2012) 167–176.

[185] J. Zhang, X. Zhao, M. Zhong, M. Yang, Y. Lian, G. Liu, S. Liu, Eur. J. Inorg. Chem. 2018 (2018) 3080–3087.

[186] M.A. Valenzuela, P. Bosch, J. Jiménez-Becerrill, O. Quiroz, A.I. Páez, J. Photochem. Photobiol. A: Chem. 148 (2002) 177–182.

[187] Y. Shen, L. Wang, Y. Wu, X. Li, Q. Zhao, Y. Hou, W. Teng, Catal. Commun. 68 (2015) 11–14.

[188] S.N. Tijare, M.V. Joshi, P.S. Padole, P.A. Mangrulkar, S.S. Rayalu, N.K. Labhsetwar, Int. J. Hydrogen Energy 37 (2012) 10451–10456.

[189] P.V. Nidheesh, R. Gandhimathi, Desalination 299 (2012) 1–15.

[190] P.V. Nidheesh, M. Zhou, M.A. Oturan, Chemosphere 197 (2018) 210–227.

[191] P.V. Nidheesh, R. Gandhimathi, Desalin. Water Treat. 52 (2013) 1872–1877.

[192] P.V. Nidheesh, R. Gandhimathi, S. Velmathi, N.S. Sanjini, RSC Adv. 4 (2014) 5698.

[193] S. Lv, X. Chen, Y. Ye, S. Yin, J. Cheng, M. Xia, J. Hazard. Mater. 171 (2009) 634–639.

[194] Y. Pang, H. Lei, Chem. Eng. J. 287 (2016) 585–592.

[195] L. Du, X. Wang, J. Wu, RSC Adv. 8 (2018) 18139–18145.

[196] A. Khataee, P. Gholami, B. Vahid, S.W. Joo, Ultrason. Sonochem. 32 (2016) 357–370.

[197] A. Zhihui, Y. Peng, L. Xiaohua, Chemosphere 60 (2005) 824–827.

[198] Y. Wang, H. Zhao, J. Gao, G. Zhao, Y. Zhang, Y. Zhang, J. Phys. Chem. C 116 (2012) 7457–7463.

[199] N. Ezzatahmadi, G.A. Ayoko, G.J. Millar, R. Speight, C. Yan, J. Li, S. Li, J. Zhu, Y. Xi, Chem. Eng. J. 312 (2017) 336–350.

[200] R.C.C. Costa, F.C.C. Moura, J.D. Ardisson, J.D. Fabris, R.M. Lago, Appl. Catal. B: Environ. 83 (2008) 131–139.

[201] O.X. Leupin, S.J. Hug, Water Res. 39 (2005) 1729–1740.

[202] S.H. Joo, A.J. Feitz, D.L. Sedlak, T.D. Waite, Environ. Sci. Technol. 39 (2005) 1263–1268.

[203] L. Wang, M. Cao, Z. Ai, L. Zhang, Environ. Sci. Technol. 48 (2014) 3354–3362.

[204] W. Liu, Z. Ai, M. Cao, L. Zhang, Appl. Catal. B: Environ. 150-151 (2014) 1–11.

[205] Z. Ai, Z. Gao, L. Zhang, W. He, J.J. Yin, Environ. Sci. Technol. 47 (2013) 5344–5352.

[206] O. Abida, M. Kolar, J. Jirkovsky, G. Mailhot, Photochem. Photobiol. Sci. 11 (2012) 794–802.

[207] Z. Zhang, X. Wang, M. Zhao, H. Qi, Carbohydr. Polym. 112 (2014) 578–582.

[208] Y. Zuo, J. Hoigné, Atmos. Environ. 28 (1994) 1231–1239.

[209] C. Zhang, L. Wang, F. Wu, N. Deng, Environ. Sci. Pollut. Res. Int. 13 (2005) 156–160.

[210] T.A. Kurniawan, W.H. Lo, Water Res. 43 (2009) 4079–4091.

[211] S. Yang, T. Xiao, J. Zhang, Y. Chen, L. Li, Sep. Purif. Technol. 143 (2015) 19–26.

[212] G. Fang, C. Zhu, D.D. Dionysiou, J. Gao, D. Zhou, Bioresour. Technol. 176 (2015) 210–217.

[213] J. Yan, L. Qian, W. Gao, Y. Chen, D. Ouyang, M. Chen, Sci. Rep. 7 (2017) 43051.

[214] L. Chen, X. Li, J. Zhang, J. Fang, Y. Huang, P. Wang, J. Ma, Environ. Sci. Technol. 49 (2015) 10373–10379.

[215] K. Wu, Y. Xie, J. Zhao, H. Hidaka, J. Mol. Catal. A Chem. 144 (1999) 77–84.

[216] J. Ma, W. Song, C. Chen, W. Ma, J. Zhao, Y. Tang, Environ. Sci. Technol. 39 (2005) 5810–5815.

[217] L. Zhou, L. Wang, J. Zhang, J. Lei, Y. Liu, Eur. J. Inorg. Chem. 2016 (2016) 5387–5392.

[218] C. Xiao, J. Li, G. Zhang, J. Cleaner Prod. 180 (2018) 550–559.

[219] A.D. Bokare, W. Choi, J. Hazard. Mater. 275 (2014) 121–135.

[220] Y. Chen, J. Gao, Z. Huang, M. Zhou, J. Chen, C. Li, Z. Ma, J. Chen, X. Tang, Environ. Sci. Technol. 51 (2017) 7084–7090.

[221] Z. Zhang, J. Sun, F. Wang, L. Dai, Angew. Chem. 57 (2018) 9038–9043.

[222] H. Wu, H. Li, X. Zhao, Q. Liu, J. Wang, J. Xiao, S. Xie, R. Si, F. Yang, S. Miao, Synth. Lect. Energy Environ. Technol. Sci. Soc. 9 (2016) 3736–3745.

[223] H. Fei, J. Dong, Y. Feng, C.S. Allen, C. Wan, B. Volosskiy, M. Li, Z. Zhao, Y. Wang, H. Sun, Nat. Catal. 1 (2018) 63.